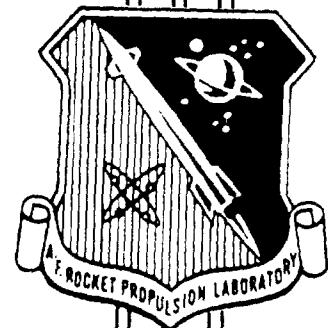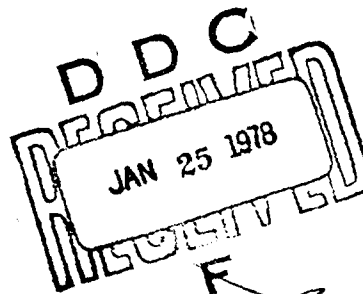**AFRPL-TR-77-56**

# VERIFICATION OF CONTAMINATION PREDICTIONS FOR MONOPROPELLANT THRUSTERS.

**FINAL REPORT,** Sep 75 – Oct 77,

## AIR FORCE ROCKET PROPULSION LABORATORY

AUTHORS:
CAPT LARRY P. DAVIS
CAPT STEVEN G. WAX

D D C

JAN 25 1978

OCTOBER 1977

**APPROVED FOR PUBLIC RELEASE**
**DISTRIBUTION UNLIMITED**

AIR FORCE ROCKET PROPULSION LABORATORY
DIRECTOR OF SCIENCE AND TECHNOLOGY
AIR FORCE SYSTEMS COMMAND
EDWARDS AFB, CALIFORNIA 93523

## NOTICES

When U.S. Government drawings, specifications, or other data are used for any purpose than a definitely related government procurement operation, the Government thereby incurs no responsibility nor any obligation whatsoever, and the fact that the Government may have formulated, furnished, or in any way supplied the said drawings, specifications or other data, is not to be regarded by implication or otherwise, or in any manner licensing the holder or any other person or corporation, or conveying any rights or permission to manufacture, use, or sell any patented invention that may in any way be related thereto.
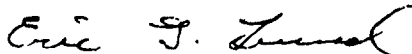
## FOREWORD

This Technical Report was prepared by the Air Force Rocket Propulsion Laboratory under Job Order No. 573009AW.
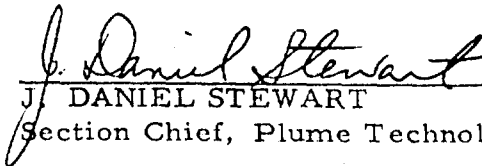
This report documents an analysis effort performed at the Air Force Rocket Propulsion Laboratory (AFRPL) to verify a portion of the CONTAM II contamination computer code against data for a 0.1 pound monopropellant hydrazine thruster. The data were obtained in the Molsink facility at the Jet Propulsion Laboratory (JPL) under AFRPL Project No. 573003AW, which was monitored by Lt Lee Witbracht (AFRPL/DYSP).

Acknowledgements are extended to the Hamilton Standard Company of Windsor Locks CT for providing the thruster and to Dr. Richard Passamaneck and Mr. Ken Baerwald of JPL for their assistance in providing minute details on all aspects of the testing procedure and data. The assistance of Dr. J. Daniel Stewart, Capt John L. Williams and Lt Eric G. Lund (AFRPL/DYSP) in critiquing the draft report and in preparing the final report are also greatly appreciated.

This report has been reviewed by the Information Office/DOZ and is releaseable to the National Technical Information Service (NTIS). At NTIS it will be available to the general public, including foreign nations. This technical report has been reviewed and is approved for publication; it is unclassified and suitable for general public release.


ERIC G. LUND, Lt., USAF
Project Manager

J. DANIEL STEWART
Section Chief, Plume Technology

FOR THE COMMANDER

JOHN I. WASHBURN, Maj, USAF
Chief, Propulsion Analysis Division

| REPORT DOCUMENTATION PAGE | | READ INSTRUCTIONS BEFORE COMPLETING FORM |
|---|---|---|
| 1. REPORT NUMBER<br><br>AFRPL-TR-77-56 ✓ | 2. GOVT ACCESSION NO. | 3. RECIPIENT'S CATALOG NUMBER |
| 4. TITLE (and Subtitle)<br><br>Verification of Contamination<br>Predictions for Monopropellant Thrusters | | 5. TYPE OF REPORT & PERIOD COVERED<br>Technical Report<br>Sep 75 - Oct 77 |
| | | 6. PERFORMING ORG. REPORT NUMBER |
| 7. AUTHOR(s)<br><br>Capt Larry P. Davis<br>Capt Steven G. Wax | | 8. CONTRACT OR GRANT NUMBER(s) |
| 9. PERFORMING ORGANIZATION NAME AND ADDRESS<br><br>AFRPL/DYSP<br>Edwards AFB CA 93523 | | 10. PROGRAM ELEMENT, PROJECT, TASK AREA & WORK UNIT NUMBERS<br><br>573003AW - Jon |
| 11. CONTROLLING OFFICE NAME AND ADDRESS<br>Air Force Rocket Propulsion Laboratory<br>Air Force System Command<br>Edwards Air Force Base, California 93523 | | 12. REPORT DATE<br>Oct 1977 |
| | | 13. NUMBER OF PAGES<br>55 |
| 14. MONITORING AGENCY NAME & ADDRESS(if different from Controlling Office)<br><br>Same as 11 | | 15. SECURITY CLASS. (of this report)<br><br>UNCLASSIFIED |
| | | 15a. DECLASSIFICATION/DOWNGRADING SCHEDULE |

16. DISTRIBUTION STATEMENT (of this Report)

Approved for public release; distribution unlimited.

17. DISTRIBUTION STATEMENT (of the abstract entered in Block 20, if different from Report)

18. SUPPLEMENTARY NOTES

19. KEY WORDS (Continue on reverse side if necessary and identify by block number)

Exhaust Plumes                          Quartz Crystal Microbalance
Plume Contamination                     Spacecraft Surfaces
Monopropellant Thruster

20. ABSTRACT (Continue on reverse side if necessary and identify by block number)

This paper represents the major results and conclusions of an AFRPL in-house analysis program set up to verify the capabilities of the monopropellant option of the CONTAM computer code for predicting plume contamination on sensitive spacecraft surfaces. The data used for verification was acquired in an AFRPL sponsored program at JPL. In that program, quartz crystal microbalance surfaces were used to measure the net deposition rate from the plume of a 0.1 lbf hydrazine thruster operating at vacuum conditions. The

CONTAM code was used to model the 0. 1 lbf thruster and to calculate the net deposition rates measured in the JPL tests. A comparison of the results indicated that the CONTAM code, while predicting the correct trends, overpredicts the plume mass deposition rates. Possible explanations for this deviation as well as a discussion of future studies to further understand the model's limitations are presented.

# TABLE OF CONTENTS

1

# LIST OF FIGURES

# LIST OF TABLES

# 1.0 INTRODUCTION

Contamination from the exhaust plume of spacecraft thrusters can pose severe problems for long-life satellite systems. Optical components (particularly if cryogenically cooled), thermal control surfaces, and solar cells are all highly susceptible to reduced performance if coated with contaminants from rocket engine exhausts. Analytical tools are needed to assess contamination problems both in the assessment of potential contamination problems during the spacecraft design phase and in the analysis of on-orbit contamination problems. The CONTAM computer code was developed by McDonnell Douglas Astronautics Corporation (MDAC) under sponsorship of the Air Force Rocket Propulsion Laboratory (AFRPL)[1] to provide these analytical tools for liquid bipropellant and monopropellant engines.

Although the CONTAM code has been in existance for a number of years, no experimental verification of the code has been accomplished. This is primarily due to the lack of applicable experimental data. Recently, however, the AFRPL sponsored a program at the Jet Propulsion Laboratory (JPL) designed to obtain mass deposition rates from the plume of a 0.1 lbf monopropellant hydrazine thruster. This data was then used by AFRPL in an attempt to assess the usability, accuracy, and deficiencies of the monopropellant portion of the CONTAM code.

This report presents a description of the AFRPL's CONTAM code evaluation effort. In addition, general provisions for assessing deposition from monopropellant hydrazine thrusters of all thrust classes are discussed.

---

(1) R.J. Hoffman, et. al., Plume Contamination Effects Prediction. The CONTAM Computer Program, Version II, AFRPL-TR-73-46, August 1973.

## 2.0 DESCRIPTION OF THE JPL EXPERIMENT

### 2.1 Overview

The data base for the evaluation of the CONTAM code is taken from mass deposition rate measurements made on the plume of a 0.1 lbf hydrazine thruster. Complete details of the JPL experiment are documented in Reference 2. For the sake of completeness, the experiment is summarized in this section.

All of the JPL tests were conducted in the JPL MOLSINK facility using a hydrazine thruster supplied by Hamilton Standard. Basically, the JPL effort consisted of three phases. First, deposition rate measurements were made with quartz crystal microbalances (QCM's). Next, a series of about 100,000 pulses was put on the engine using a combination of duty cycles. Finally, additional deposition rate measurements were made to assess the aging effect of the 100,000 pulses on contamination.

The deposition rate measurements were made using five QCM's mounted in the far field of the plume at angles of approximately $0^{\circ}$, $\pm 15^{\circ}$, and $\pm 30^{\circ}$ relative to the plume centerline. The thruster was fired with monopropellant grade hydrazine [MIL-P-26536C, [1]]. Table I is a summary of the JPL deposition rate tests. Table II is a description of the aging test series performed by JPL on the engine.

### 2.2 Test Data

The QCM measures mass deposition by equating a change in frequency to a change in mass. By calculating the slope of the mass change with time, one can obtain a mass deposition rate. JPL's frequency measurements were made every 120 seconds and thus the mass deposition rate measurements are actually average rates over a period of about twelve pulses, including on time and off time.

---

(2)  R. Passamaneck and J.E. Chirivella, "Contamination Measurements for a 0.1 lbf. Monopropellant Thruster," JANNAF Ninth Plume Technology Convention, February 1976.

4

TABLE I

## SUMMARY OF JPL DEPOSITION RATE TESTS

| Nomenclature | Duty Cycle sec on/sec off | Bed Temperature $^{\circ}K$ | QCM Temperature $^{\circ}K$ |
|---|---|---|---|
| Baseline | 0.1/10 | 478 | 144, 172, 200 |
| Baseline (with Heat Shield on Engine) | 0.1/10 | 478 | 106, 144, 172, 200 |
| Short Pulse | 0.025/5 | 478 | 144, 172, 200 |
| Long Pulse | 0.2/20 | 478 | 144, 172, 200 |
| $294^{\circ}K$ Cat Bed | 0.1/10 | 294 | 172 |
| $367^{\circ}K$ Cat Bed | 0.1/10 | 367 | 172 |
| Baseline (Water added)* | 0.1/10 | 478 | 144, 172, 200 |
| Baseline (aged)** | 0.1/10 | 478 | 144, 172, 200 |
| $589^{\circ}$ Cat Bed*** | 0.1/10 | 589 | 172 |

* $H_2O$ mass fraction = 0.0181, all other $H_2O$ mass fractions = 0.0071

** After 100,000 pulses (see Table II); since model does not account for aging, this case was not run analytically.

*** This case was not run analytically.

During the mass deposition tests, JPL measured thruster wall temperature to determine when equilibrium had been reached. During the aging tests, chamber pressure (Pc) was also monitored. Photographs of the Pc traces displayed on an oscilloscope provided the peak pressures for the aging tests.

## TABLE II

### JPL AGING TESTS

| SERIES # | Time on (sec) | Time off (sec) | No. Pulses |
|----------|---------------|----------------|------------|
| 1 | 0.020 | 120 | 50 |
| 2 | 0.035 | 120 | 50 |
| 3 | 0.050 | 120 | 50 |
| 4 | 0.100 | 120 | 50 |
| 5 | 0.250 | 300 | 5 |
| 6 | 0.015 | 15 | 100 |
| 7 | 0.500 | 120 | 10 |
| 8 | 1.0 | 120 | 10 |
| 9 | 0.125 | 12.375 | 1000 |
| 10 | 0.04 | 1.16 | 5000 |
| 11 | 0.04 | 0.40 | 7000 |
| 12 | 1.0 | 10.0 | 100 |
| 13 | 0.10 | 0.90 | 6000 |
| 14 | 0.075 | 0.525 | 6000 |
| 15 | 0.090 | 0.100 | 7000 |
| 16 | 0.020 | 0.020 | 1000 |
| | | TOTAL* | 33425 |

* Series 1-16 is repeated three times for ≈100,000 total pulses.

# 3.0 CONTAM MODEL IMPLEMENTATION

## 3.1 Model Description

The CONTAM code for monopropellant hydrazine thrusters actually consists of a series of four separate routines.[1] The N2H4 routine calculates the end-of-bed properties suitable for input into the flowfield parts of the code. The MULTRAN routine performs a method-of-characteristics calculation of the nozzle and plume flowfield characteristics following a transonic analysis through the throat. A one-dimensional chemical kinetics calculation along the MULTRAN, pressure-defined streamlines is then performed with the KINCON routine. This routine also includes the capability to predict plume condensation of a single species. The resultant velocities, densities, and species concentrations along streamlines are used to calculate the mass flux points within the plume. The SURFACE routine calculates deposition ra᷉s to the spacecraft surface and resultant changes in surface properties. Since the emphasis of this work was placed on mass deposition rates as a function of surface temperature, this routine was not exercised. When the CONTAM code is used for bipropellant engines, a transient combustion chamber code (TCC) is substituted for N2H4, while the other codes remain the same. The data base for this effort was a monopropellant engine and thus TCC is not discussed in this report.

Since SURFACE was not used, the net deposition rate predicted at the QCM surface had to be calculated by subtracting the evaporation rate of each species from the plume deposition predicted by N2H4, MULTRAN, and KINCON. Following is a discussion of each model and of the technique used in calculating net deposition rate.

## 3.2 N2H4 Routine

The N2H4 code is a one-dimensional, non-steady state model which calculates end-of-bed properties using finite difference solutions of mass transfer, heat transfer and chemical reaction rate equations. In actuality, N2H4 is taken

with only minor modification from the transient model developed for NASA by
A. S. Kesten. [3], [4], [5] A very complete discussion of the equations and limitations used in the transient model is detailed in the references. The reports also include the derivation or references for the physical properties used in the model.

Table III is a listing of the input parameters used in the "baseline" test case. The steady-state parameters are obtained from a steady-state model developed by Kesten. [6], [7] The geometrical inputs for the steady state model are the same as those for N2H4. Since N2H4 estimates by extrapolation to steady-state conditions, the running of the steady state model is essential. It is not, however, included in the CONTAM code and must be obtained separately.

During the course of running N2H4 several difficulties were encountered. The most serious of these was the way in which N2H4 modeled the thruster's thermal characteristics. N2H4 does not contain any provisions for a heat shield nor for cooling to a space temperature different than the temperature to which

(3)  A. S. Kesten, Analytical Study of Catalytic Reactors for Hydrazine
     Decomposition. United Aircraft Research Laboratories Report
     G910461-24, Second Annual Progress Report, Contract NAS-7-458, May
     1968.

(4)  A. S. Kesten, Analytical Study of Catalytic Reactors for Hydrazine
     Decomposition. United Aircraft Research Laboratories Report
     H910461-38, Third Annual Progress Report, Contract NAS-7-458, May 1969.

(5)  D. B. Smith, E. J. Smith, and A. S. Kesten, Analytical Study of Catalytic
     Reactors for Hydrazine Decomposition. United Aircraft Research
     Laboratories Report H910461-37, Computer Program Manual, Transient
     Model, May 1969.

(6)  A. S. Kesten, Analytical Study of Catalytic Reactors for Hydrazine
     Decomposition. United Aircraft Research Laboratories Report F910461-12,
     First Annual Progress Report, Contract NAS-7-458, May 1967.

(7)  D. B. Smith, E. J. Smith, and A. S. Kesten, Analytical Study of Catalytic
     Reactors for Hydrazine Decomposition. United Aircraft Research Labora-
     tories Report G910461-30, Computer Programs Manual, One-Dimensional
     and Two-Dimensional Steady State Models, August 1968.

8

# TABLE III

## N2H4 INPUTS, BASELINE CASE

| QUANTITY | DESCRIPTION | VALUE | UNITS+ |
|---|---|---|---|
| **Steady-State Parameters** | | | |
| GOSS | Steady State Mass Flow Rate | 0.11772 | lbm/ft$^2$-sec |
| MBSS | Steady State Molecular Weight | 12.525 | lbm/lb-mole |
| PSS | Steady State Chamber Pressure | 81.04 | psia |
| TSS | Steady State Temperature | 2037 | $^O$R |
| TVAP | Hydrazine Vaporization Temp. | 804 | $^O$R |
| HIV | **Enthalpy** of Liquid Vapor Interface | 709.2 | BTU/lbm |
| **Operational Variables** | | | |
| F | Flow Rate Through Buried Inj. | 98.1 | lbm/ft$^3$-sec |
| HF | Enthalpy of Feed | 78. | BTU/lbm |
| PF | Pressure of Feed | 114. | psia |
| TA | Ambient Temperature | 860. | $^O$R |
| TPi | Initial Catalyst Temperature | 860. | $^O$R |
| | Initial Concentrations of $N_2H_4$, $NH_3$, $H_2$, $N_2$ | $1.0 \times 10^{-9}$ | lbm/ft$^3$ |
| TLIQ | Temperature of Liquid Hydrazine | 860. | $^O$R |
| TS | Background Temperature | 36 | $^O$R |
| | Duty Cycle | .1 sec on/ 10 sec off | |
| PCI | Initial Chamber Pressure | 0.001 | psia |
| **Chamber & Catalyst Characteristics** | | | |
| AC | Cross Sectional Area of Reaction | $3.98 \times 10^{-4}$ | ft$^2$ |
| MW | Chamber Wall Thermal Mass | 0.01378 | lbm |
| VC | Free Volume of Chamber | $4.95 \times 10^{-6}$ | ft$^3$ |
| AW | Chamber Wall Specific Heat | 0.1 | BTU/lbm-$^O$R |
| HA | Forced Convection Heat Transfer Coefficient | 0. | BTU/ft$^2$-sec-$^O$R |
| HA1 | Natural Convention Heat Transfer | 0. | BTU/ft$^2$-sec-1.25-$^O$R |
| HA2 | Radiative Heat Transfer Coefficient | $1.5 \times 10^{-13}$ | BTU/ft$^2$-sec-$^O$R$^4$ |
| AS | Heat Shield Area | (No shield) | ft$^2$ |
| Z | Length of Bed | 0.0358 | ft |
| Z0 | Axial Distance to End of Buried Injector | 0.0108 | ft |
| RADT | Radius of Catalyst Particles (25-30 Mesh) | $8.98 \times 10^{-4}$ | ft |
| SURFT | Catalyst Particle Surface Area/Unit Volume of Bed | 2070 | ft$^2$/ft$^3$ |
| VOIDT | Interparticle Void Fraction | 0.38 | ----- |

+ Quantities are in units required for program input.

the catalyst bed is heated. These provisions were added by AFRPL since they were required for modeling the JPL tests. In addition, original estimates for natural convection and radiation coefficients gave a poor thermal fit to the baseline data. Since the purpose of this effort was to predict deposition and not wall temperature, it was decided to approximate the baseline thermal response empirically using only radiation. A radiation coefficient which gave a close fit to the baseline thermal response was found (Table III) and used throughout. Figure 1 shows the baseline fit.

When N2H4 is operated in the pulse mode, the peak pressure predicted for a given pulse is higher than that for the previous pulse. This difference decreases gradually until finally each pulse is predicted to be identical to the next, and for the purpose of comparison with experiment, is considered to be "steady-state". Figure 2 shows a comparison of the pressure traces for pulses 1, 5, 45, and 60 of the baseline case. After pulse 45, the traces are nearly identical. Upon re-examining Figure 1, it can be observed that the temperature also levels off after about 45 pulses (450 seconds). Past pulse 60, the model predicts no change in engine parameters, and it is these steady-state parameters that were used to develop input for the subsequent contamination prediction routine. However, N2H4 predicts values as a function of time throughout a pulse while MULTRAN and KINCON require properties at a discrete time. The simplest technique is to average the parameters over the entire pulse. For chamber pressure and temperature the average is obviously an acceptable approach. In the "steady-state" regime (past pulse 60) the temperature is fairly constant. Also, the pressure rise and fall are so fast that the chamber pressure is essentially at the average for the entire pulse. Conversely, the end-of-bed species concentrations, essential for calculation of mass flux, vary quite a bit and thus the accuracy of the averaging technique for these properties has to be evaluated. The validity of this technique is discussed in the Transient Effects section (3.6).
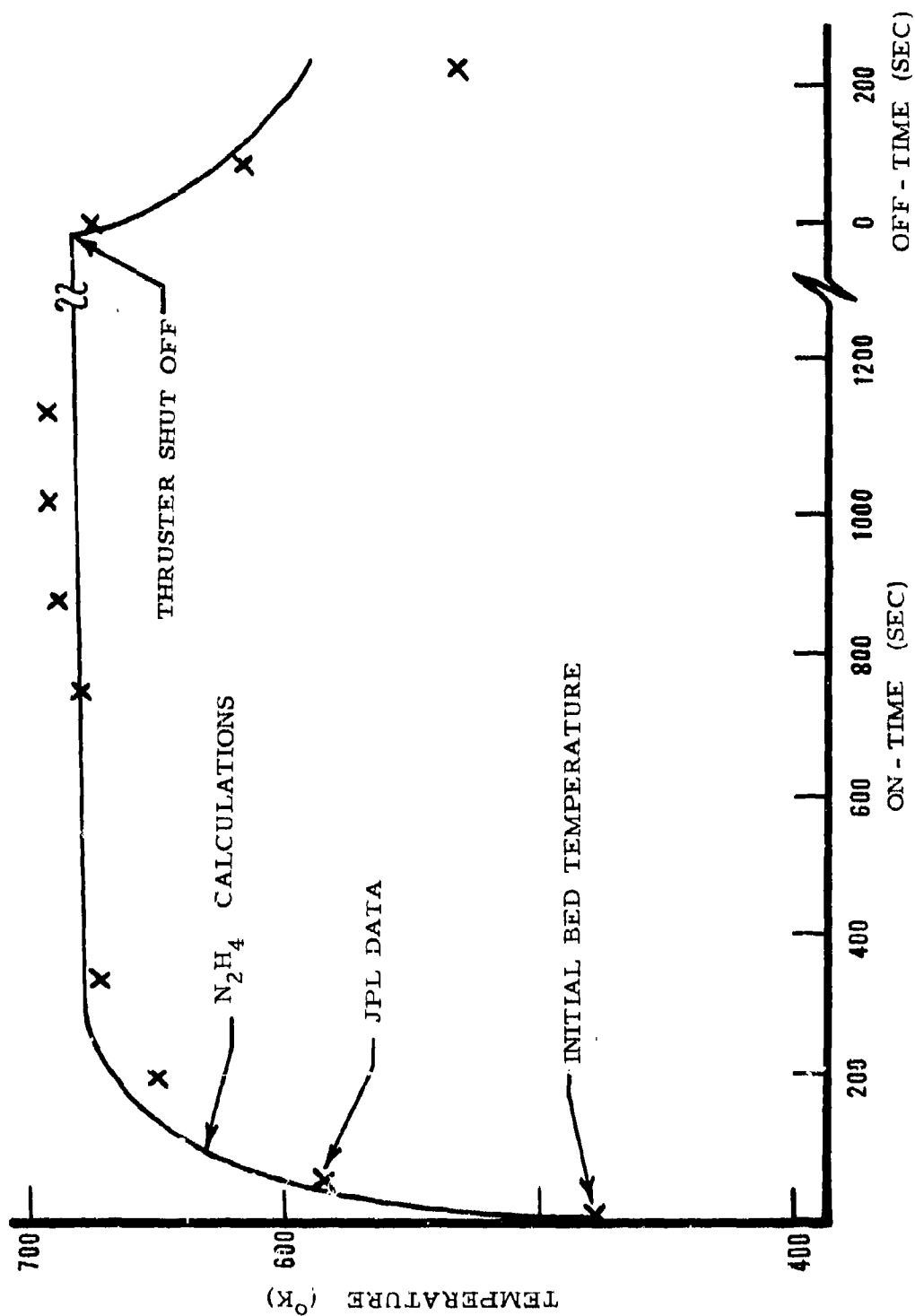
Figure 1. Baseline Thermal Profile Matching
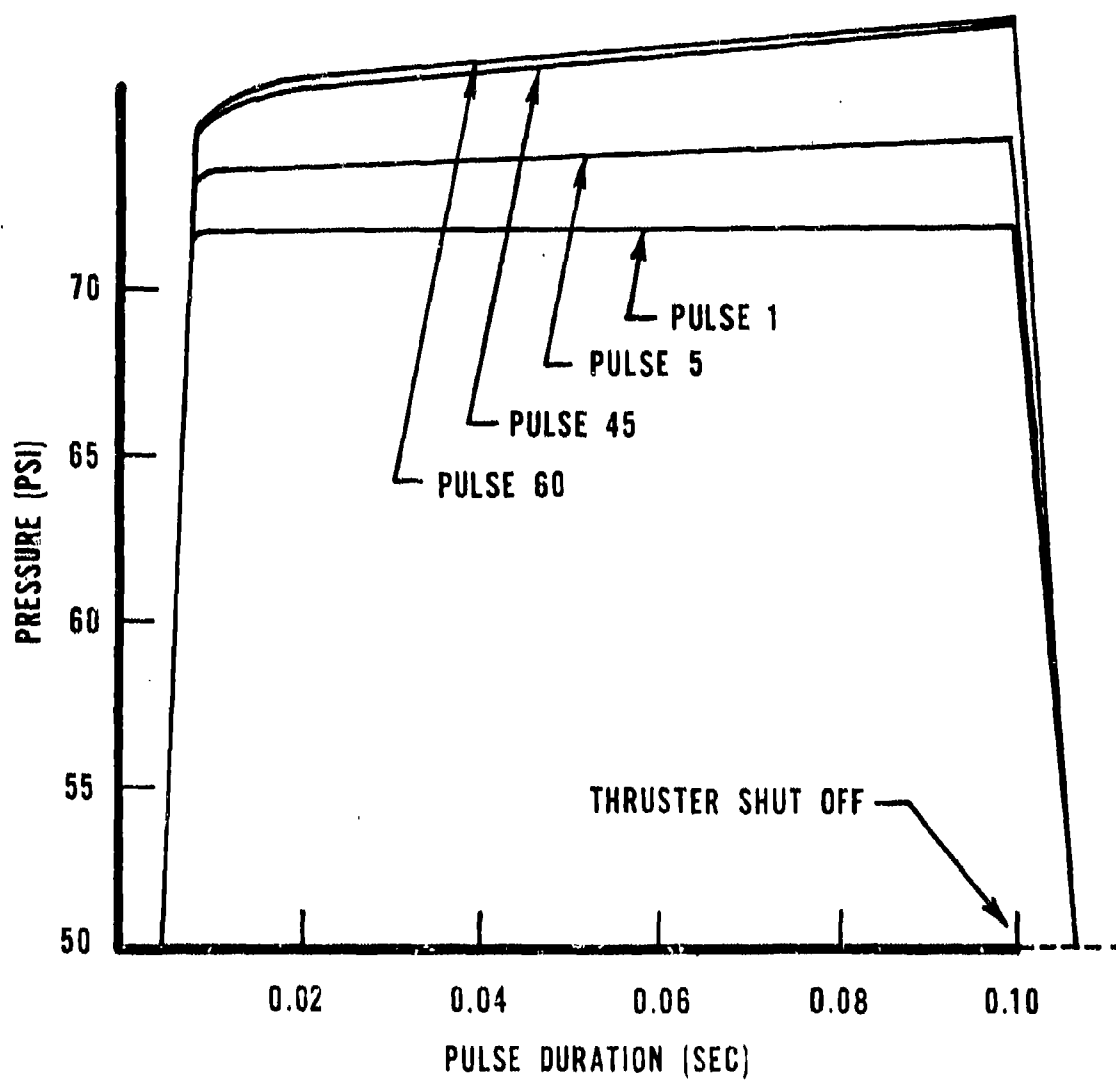
Figure 2. Pressure Versus Time for Selected Baseline Pulses

12

Table IV shows the inputs to <u>MULTRAN</u> and <u>KINCON</u> that were calculated by <u>N2H4.</u> Since the number of pulses for the model to reach steady state varied with conditions, the pulse used for calculations is also indicated. It should be noted that the "water added" inputs were taken from the baseline case and adjusted for the higher mass fraction of water in the propellant.

TABLE IV

<u>N2H4 - CALCULATED INPUTS TO MULTRAN AND KINCON</u>[+][‡]

| CASE (Pulse for steady state) | Specific Heat Ratio | Chamber Pressure PSIA | Chamber Temp R | MASS FRACTION[*] | | | |
|---|---|---|---|---|---|---|---|
| | | | | $NH_3$ | $N_2$ | $H_2$ | $N_2H_4$ |
| Baseline (60) | 1.1941 | 59.46 | 1225 | .51354 | .46365 | .01571 | $4 \times 10^{-4}$ |
| Short Pulse (60) | 1.1876 | 22.47 | 1009 | .52128 | .46023 | .01139 | $1.7 \times 10^{-4}$ |
| Long Pulse (40) | 1.2131 | 66.80 | 1225 | .45484 | .51691 | .02115 | $1.0 \times 10^{-3}$ |
| 70° Bed (40) | 1.1921 | 58.96 | 1143 | .53182 | .44424 | .01684 | $2.3 \times 10^{-4}$ |
| 200° Bed (60) | 1.1917 | 59.17 | 1178 | .53003 | .44673 | .01614 | $2.5 \times 10^{-4}$ |
| Water Added | Same as increase | Baseline except water | $H_2O$ Flux was adjusted for 1% | | | | |

+ quantities were averaged over total pulse

‡ quantities are in units required for program input

* mass fraction of $H_2O$ = .0071 except for "water added" case, where $H_2O$ mass fraction = .0181

## 3.3 MULTRAN Routine

The <u>MULTRAN</u> routine of <u>CONTAM</u> performs a method of Characteristics (MOC) calculation following a transonic analysis through the throat. Inputs to

the MULTRAN code from N2H4 have already been discussed in Section 3. 2. The engine design parameters used for MULTRAN input are presented in Table V. The actual radius of curvature, 2. 0, had to be changed to 2. 667 since the code was not designed to handle small radii of curvature. From a sensitivity study of this parameter, varying it over the range that the code would allow, it can be concluded that the results are insensitive to this change.

TABLE V

MULTRAN INPUTS

| Quantity | Description | Values | Units+ |
|----------|-------------|--------|--------|
| THID | Inlet Angle | 30 | Degrees |
| RT | Throat Radius | .00125 | Feet |
| RRT* | Throat Radius of Curvature | 2. 667 | Normalized to Throat Radius |
| EPS | Nozzle Area Ratio (Core) | 55. 3 | -- |

\* Actual Value = 2. 0, see text.

+ Quantities are in units required for program input.

In the operation of MULTRAN, it was found that the model would not calculate values beyond a distance of 30 - 50 throat radii, nor would the model accept a Prandtl-Meyer expansion angle of greater than 70°. Upon completion of the MOC calculation, the code sets up a series of pressure defined streamlines that are subsequently read into KINCON. Figure 3 shows a typical plot of MULTRAN streamlines. If the 99. 99% streamline of that figure is examined, it can be seen that the points (shown by circles) do not all fall on the expected line. Thus the true angle that the streamline would strike a surface a large distance away from the thruster could not be accurately determined. This plus the inability of the model to expand the plume beyond 70° had a great effect on the off-centerline calculations. This effect will be discussed further in Sections 4 and 5.
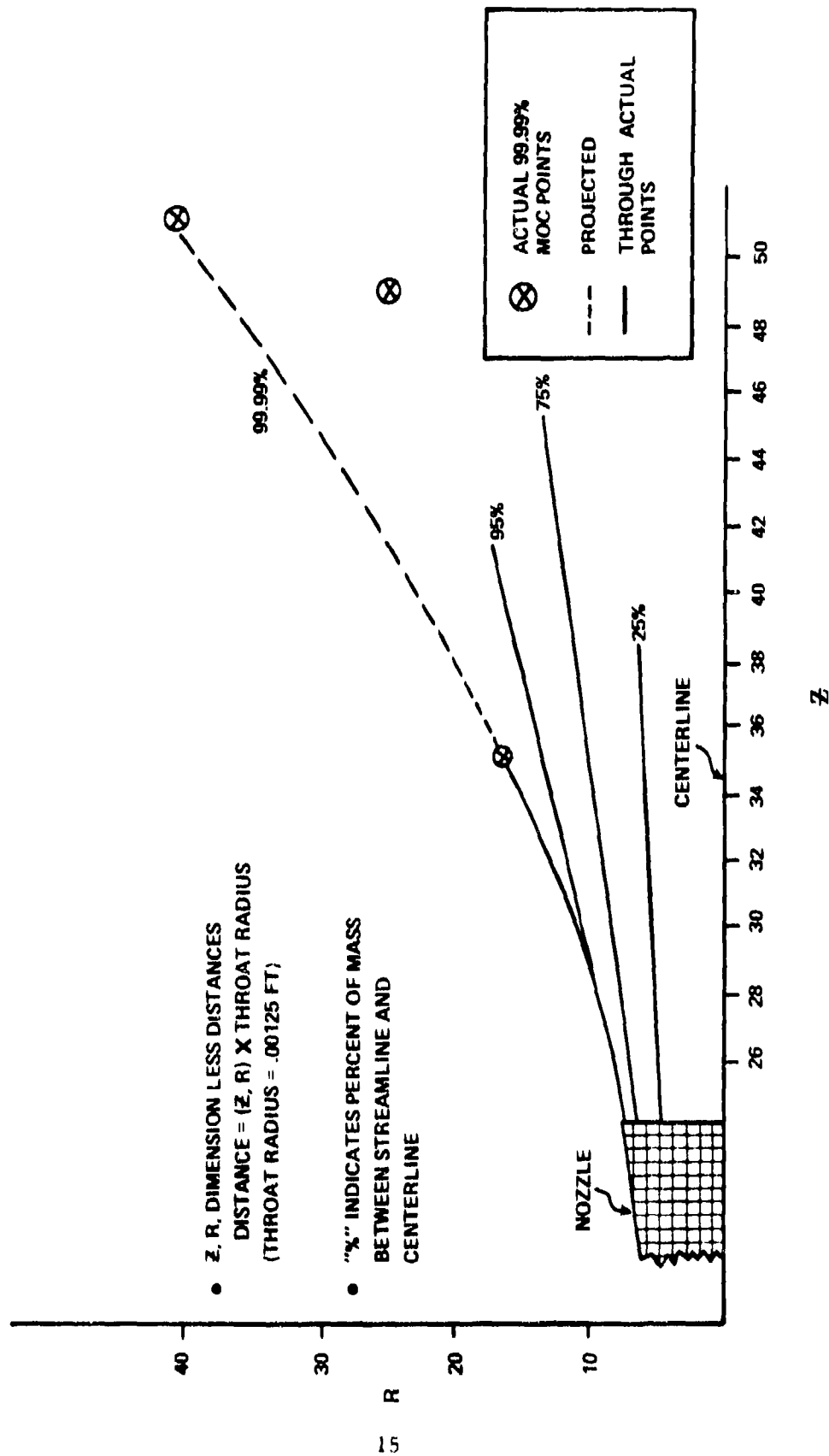
14

Figure 3. MULTRAN Generated Streamlines

15

## 3.4 KINCON Routine

KINCON was used as described in the CONTAM manual, with the pressure-defined streamlines from MULTRAN and species mass fraction produced by N2H4 as input, with the following exceptions: (a) hydrazine was not included in the KINCON calculation because data for it is not included in the standard KINCON thermodynamic library; (b) water was added to the flow field in the same amount as was found in the propellant. (The nitrogen concentration was adjusted slightly to make the mass fractions sum to one.) No chemical reactions were included in the calculation, except for the dummy reaction $NH_3 \rightarrow NH_3$ (the program requires at least one reaction). The species mass fractions were thus frozen at the chamber exit values. This approximation should be quite good because of the relatively low pressures and temperatures in the nozzle and plume compared with the chamber conditions. Eventhough hydrazine was not included as part of the flow field calculation itself, it was added back into the composition at its end-of-bed value for the mass deposition rate calculation. Although KINCON also has the capability of calculating condensation of one species in the flow field, this option was not exercised for this work.

## 3.5 Calculation of Net Deposition Rates

The output from KINCON was used to obtain mass fluxes at points along each streamline from the equation:

$$\dot{m}(r) = \rho(r) \cdot V(r) \qquad (1)$$

where:  $\rho(r)$ = the gas density at r in $g/cm^3$

$V(r)$ = the gas velocity at r in cm/sec

$r$ = the distance along the streamline from the throat in cm

$\dot{m}(r)$ = the mass flux per unit area at r in $g/cm^2$ - sec

16

This mass flux per unit area can be converted to a mass flux per unit solid angle via the equation:

$$\frac{d\dot{m}}{d\Omega}(r) = \dot{m}(r) \cdot r^2 \cos\phi \qquad (2)$$

where: $\frac{d\dot{m}}{d\Omega}(r)$ = the mass flux per unit solid angle in g/sec-steradian

$\phi$ = the angle between the direction of flow and the normal of the surface through which the flux is calculated.

In principle, $\dot{m}(r)$ can be calculated at positions along any streamline to a distance where the QCM's are located to compare with the QCM data. In practice, it is found that $\frac{d\dot{m}}{d\Omega}(r)$ becomes constant at relatively close distances from the exit plane compared with the distance to the QCM's, thus demonstrating that the plume far field is similar to a source flow. The calculation with KINCON is only done out to the point where $\frac{d\dot{m}}{d\Omega}(r)$ becomes constant. The mass flux, $\dot{m}(r)$, can be found by solving equation (2) at any location r. The angle $\phi$ was taken to be $0^{\circ}$ since the QCM data had been corrected for the inclination effect. Once $\dot{m}(r)$ at the QCM is calculated, the deposition rate for each contaminant species is calculated from:

$$\dot{m}_i = X_i \dot{m} \qquad (3)$$

where: $\dot{m}_i$ = the mass deposition rate for species i in g/cm$^2$ - sec

$X_i$ = the mass fraction of species i in the flow field

$\dot{m}$ = the total mass flux per unit in g/cm$^2$ - sec

The mass flux predicted by CONTAM is the flux for the total run time; the time for which the chamber pressure was above its initial value. To calculate the mass flux rate hitting the crystal, it is necessary to average the flux over the sum of the on and off time (See Appendix A).

17

The evaporation rate for each species $\dot{m}_{e_i}$ was calculated using the expression from reference 8:

$$\dot{m}_{e_i} = (5.83 \times 10^{-2}) \, Y P_v \left(\frac{MW}{T}\right)^{\frac{1}{2}} \tag{4}$$

where: $\dot{m}_{e_i}$ = the evaporation rate in $g/cm^2$ - sec of species i

$Y$ is an accomodation coefficient (assumed = 1)

$P_v$ = equilibrium vapor pressure in Torr of species i at temperature T

MW = molecular weight of species i in g/mole

$T$ = QCM temperature in $^{\circ}K$

The choice of unity as the value of the accomodation coefficient is equivalent to assuming that any deposit equilibrates to the QCM temperature. Also, this expression assumes zero external pressure and is not valid for external pressures of about the same magnitude as the vapor pressure or larger. If this condition occurs, the actual evaporation rate will be smaller than that calculated with equation 4. However, in the experiment where the vacuum chamber was constantly cryopumped, equation 4 should be valid.

From the CRC Handbook of Chemistry and Physics[9], the vapor pressure for solid ammonia was represented by:

$$\log P_v = \frac{-1630.15}{T} + 9.9974 \tag{5}$$

where: $P_v$ = ammonia vapor pressure in torr

$T$ = Temperature in $^{\circ}K$

(8) R. J. Hoffman, et. al., Op. Cit., page 250.

(9) Handbook of Chemistry and Physics, The Chemical Rubber Company, Cleveland, Ohio, 1967 - 68 Edition.

This equation is an empirical curve fit valid for temperatures between $146^\circ K$ and $195^\circ K$. Ice vapor pressure data was obtained from the equation:

$$\text{Log } P_v = \frac{-2481.604}{T} + 3.5721988 \log T - 3.97203 \times 10^{-3} \times T - 1.7649 \times 10^{-3}$$

$$T^2 + 1.901973 \qquad (6)$$

where: $P_v$ = ice vapor pressure in torr

$T$ = temperature in $^\circ K$

This equation was obtained from a theoretical derivation[10] which has been shown to match experimental data between $173^\circ K$ and $373^\circ K$ to within the experimental accuracy. Hydrazine vapor pressure was obtained from a correlation of vapor pressure using a three constant expression, $\ln P_v = A - \frac{B}{T+C}$, where C is an empirical function of the critical temperature and A and B are calculated from known vapor pressures. The equation is as follows:

$$\ln P_v = 13.3828 - \frac{3273}{T - 80.65} \qquad (7)$$

The net deposition for each species is then calculated as

$$\dot{m}_{net\ i} = \dot{m}_i - \dot{m}_{e_i} \qquad (8)$$

If $\dot{m}_{net\ i} < 0$ then $\dot{m}_{net\ i} = 0$. The total net deposition is calculated by summing over all species considered.

$$\dot{m}_{net} = \sum_{i=1}^{N} \dot{m}_{net\ i} \qquad (9)$$

For the purpose of this analysis only $N_2H_4$, $NH_3$, and $H_2O$ are considered. The evaporation rates of $H_2$ and $N_2$, the other species of $N_2H_4$ decomposition are too high to deposit at the crystal temperatures used in this analysis.

(10) G. Jancso, et. al., J. Phys. Chem., 1970, 74 (15), 2984-9.

## 3.6 Transient Effects

As mentioned in the preceeding sections, the N2H4 model generates inputs as a function of time during a pulse. To use MULTRAN and KINCON, it was necessary to average these inputs over the pulse duration. The validity of this technique was assessed by comparing the average of mass fluxes calculated for several times during a pulse with the mass flux calculated from average pulse properties. Based on the results of this comparison, (see Figure 4), only one set of calculations was needed for each pulse. A similar check of the individual mass fluxes for each specie also indicated that the pulse average quantity is a reasonable value, except perhaps for hydrazine which has the most fluctuation during a given pulse. The approximation in all cases can be expected to be better for longer pulses when the average is closer to the statistical mode.

As the change from pulse to pulse of N2H4 predicted parameters begins to become minimal (see Section 3.2), so too do the differences in CONTAM predicted mass deposition rates. Figure 5 indicates this for the baseline case. It can be seen that there is a gradual decline in the deposition rate over the first 10 - 15 pulses. By pulse 60, the deposition rate has leveled, and a "steady state" is obtained. This deposition rate was used to calculate the net deposition rates for comparison with JPL data. Since JPL measured QCM frequency only every 120 seconds (approximately 12 pulses), it was impossible to compare the CONTAM predictions during early pulses with JPL's. In fact, JPL's data comes from readings taken after at least 100 pulses. In making the comparisons, the initial CONTAM transient must be ignored. Since changes in deposition rate and not absolute mass are being measured, this limitation should not be serious.
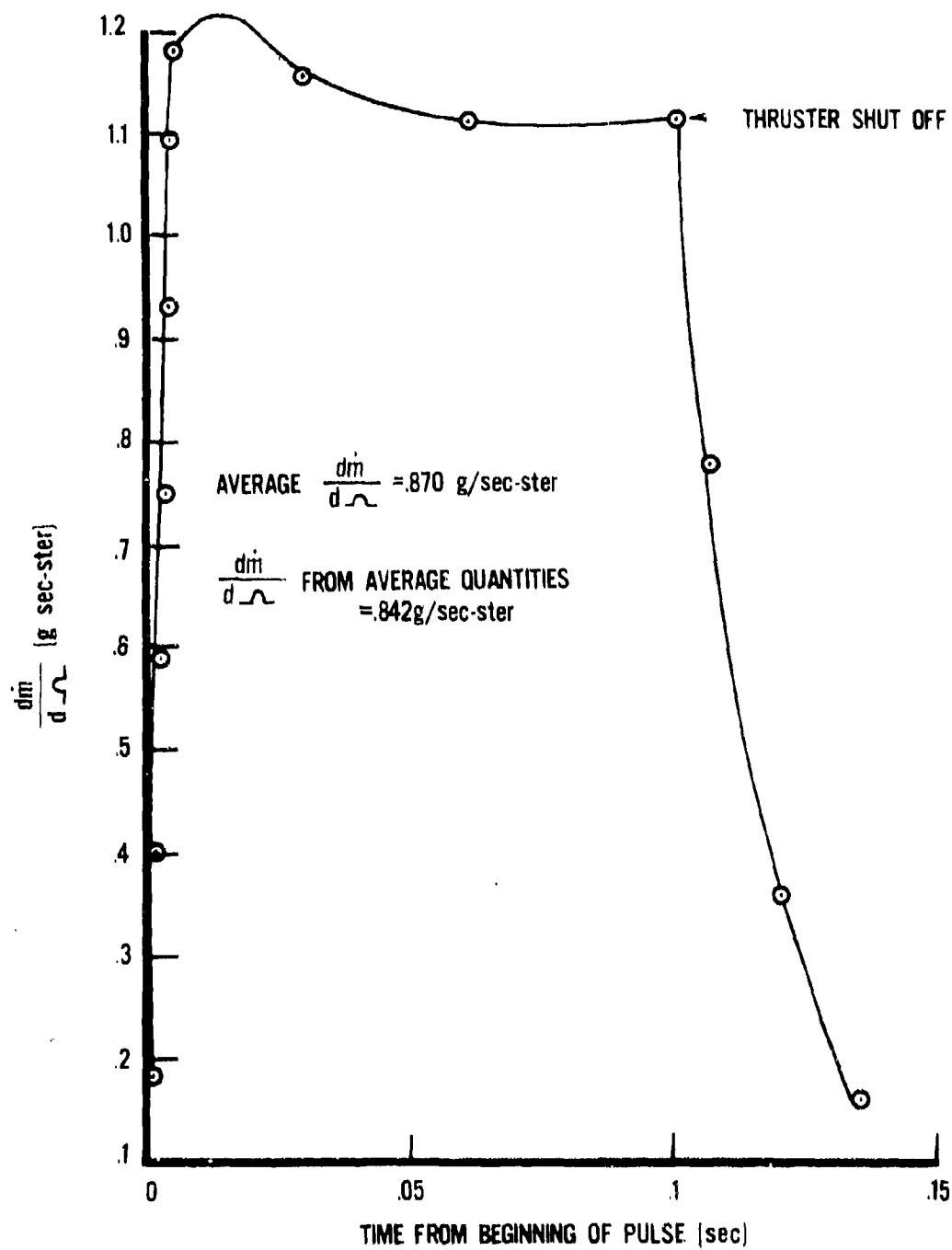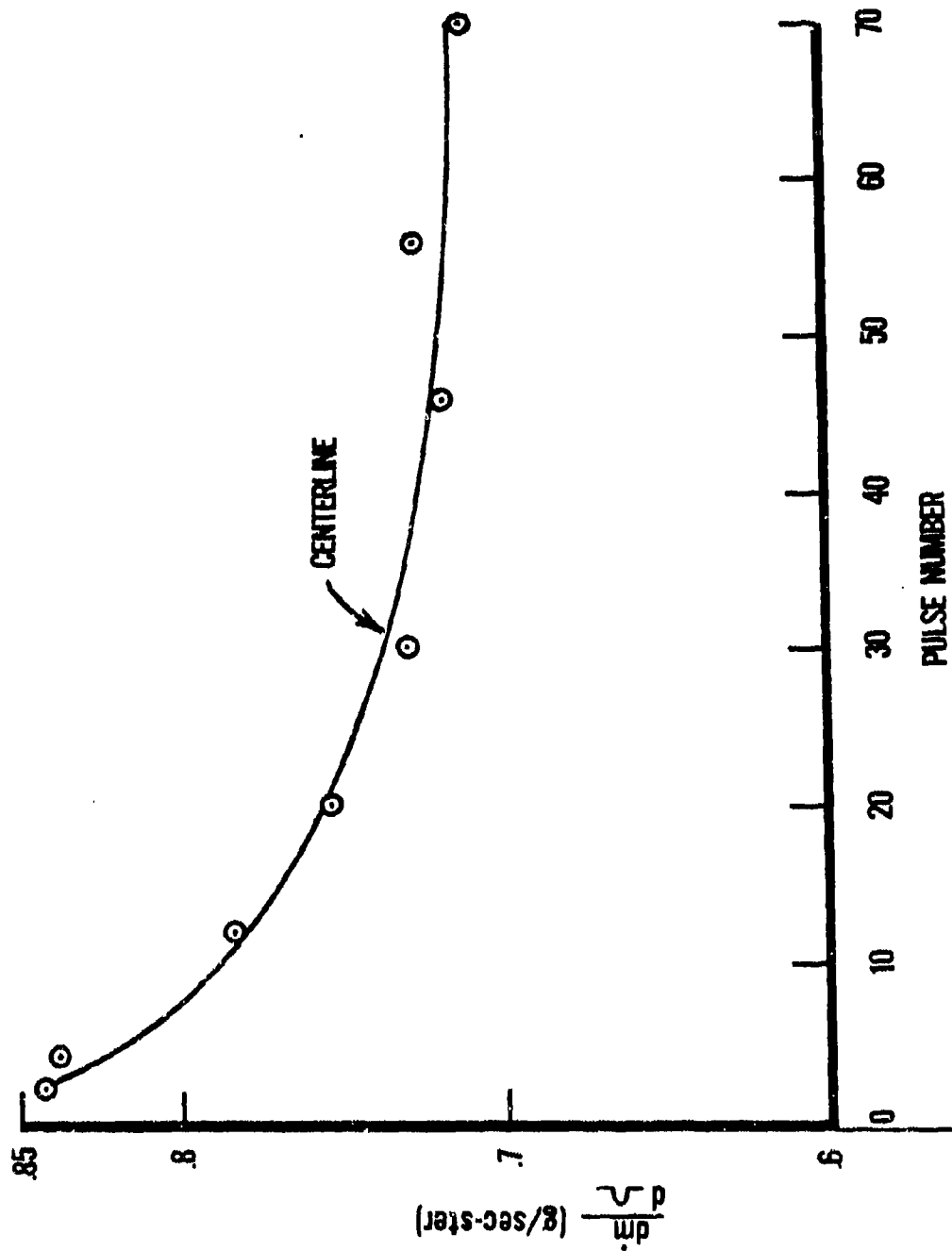
20

Figure 4. $\frac{d\dot{m}}{d\Omega}$ Vs. Time

21

Figure 5. $\frac{d\dot{m}}{d\Omega}$ Vs. Pulse Number

# 4.0 PRESENTATION OF RESULTS

## 4.1 N2H4 Data Comparison

Although the comparison between JPL measured and <u>CONTAM</u> predicted mass deposition rates is of primary concern in this effort, the engine data taken by JPL during the tests (see Section 2.2) offered a chance to evaluate the output from the <u>N2H4</u> code.

Table VI shows a comparison between experimental and predicted values of peak pressure for those aging duty cycles (see Table II) for which <u>N2H4</u> was run. It should be remembered that JPL's pressure value had to be interpolated from photographs of oscilloscope traces. Thus, the agreement for all but series No. 1 is reasonable. Based on the short on-time, one must assume that the reported experimental value for series No. 1 is in error.

Table VII presents the maximum and minimum temperatures recorded by JPL for six of the aging series (see Table II) and the model predictions for these values. The correlation between the predicted and experimental maximum temperatures is good, (0.96) although for long off times (>120 seconds) or for long on times (>.15 second) the final wall temperature is overestimated. This is understandable if one considers the empiricism used to model wall cooling (see Section 3.2). Figure 6 compares several <u>N2H4</u> predicted wall temperature profiles with JPL measured data. When the particular duty cycle was close to the baseline (0.1 on/10 off) the fit was good (see Figure 1). As the duty cycle varied from the baseline case the fit became poorer.

## 4.2 Centerline Mass Deposition Rates:

The centerline mass deposition rates predicted by <u>CONTAM</u> for all of the JPL cases modeled are presented in Table VIII. It should be remembered that these are the predicted rates at which mass <u>strikes</u> the QCM. To calculate the net deposition rate, one must subtract the evaporation rate of each species from its deposition rate; the values shown in Table VIII are independent of QCM temperature. Appendix A presents a sample calculation.

## TABLE VI

### PEAK PRESSURE COMPARISON

| Series # | Duty Cycle on/off (sec) | Experimental Peak Pressure (PSIA) | Predicted Peak Pressure (PSIA) |
|----------|------------------------|-----------------------------------|--------------------------------|
| 1 | .02/120 | 95.0 | 70.0 |
| 2 | .035/120 | 72.5 | 71.2 |
| 3 | .05/120 | 80. | 71.4 |
| 4 | .10/120 | 72.5 | 71.8 |
| 5 | .25/300 | 72.5 | 73.6 |

## TABLE VII

### TEMPERATURE RANGE COMPARISON

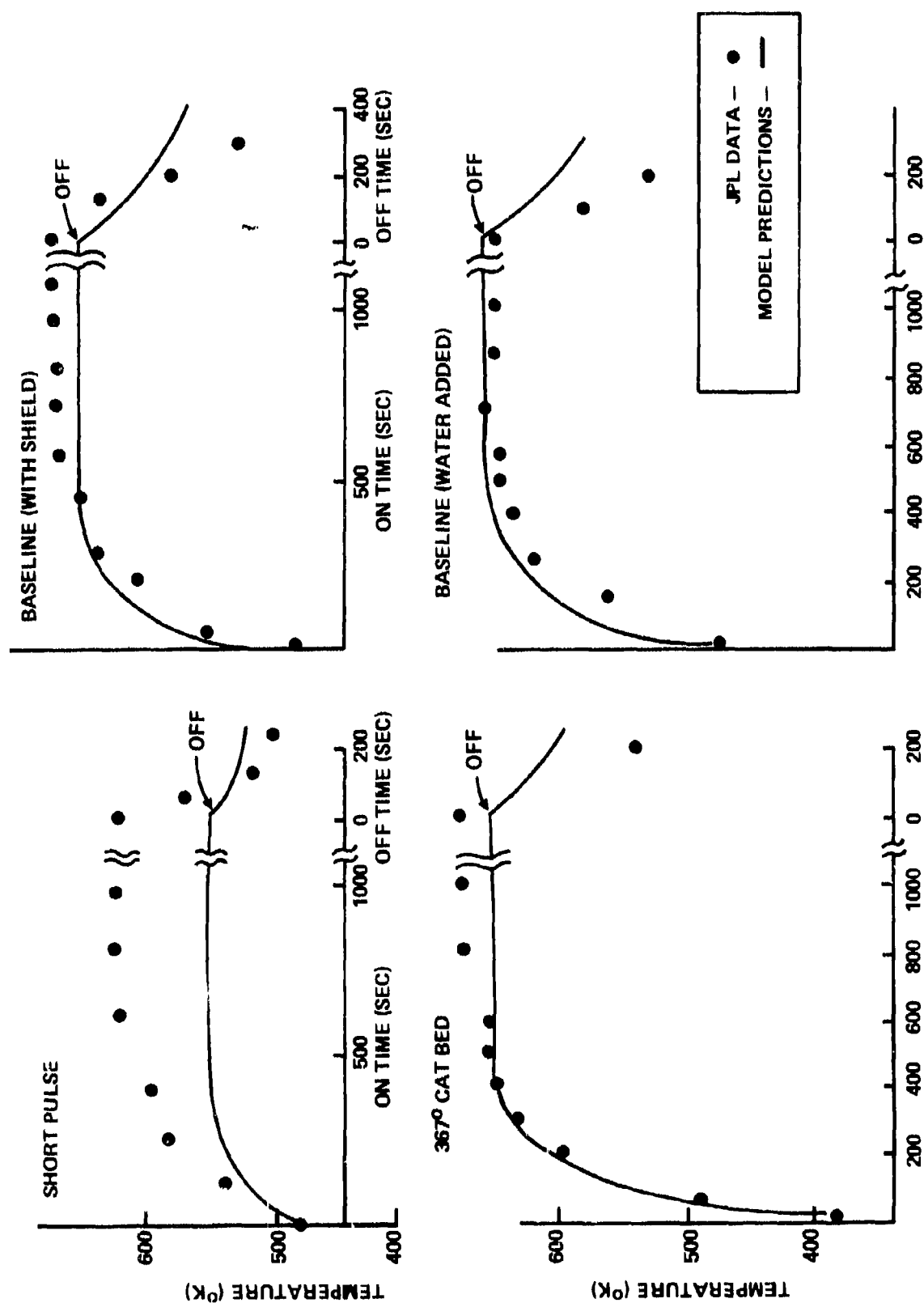| Series # | Duty Cycle | Experimental ($^{O}R$) | | Predicted ($^{O}R$) | |
|----------|-----------|------|------|------|------|
| | | MAX | MIN | MAX | MIN |
| 1 | 02/120 | 873 | 860 | 906 | 861 |
| 2 | .035/120 | 880 | 860 | 904 | 860 |
| 3 | .050/120 | 881 | 860 | 908 | 860 |
| 4 | .10/120 | 891 | 860 | 889 | 862 |
| 5 | .25/300 | 923 | 860 | 964 | 900 |
| 8 | 1.0/120 | (1)* 1038 | 860 | 1056 | 999 |
| | | (2)* 1043 | 889 | 1152 | 1065 |
| | | (3)* 1045 | 890 | 1203 | 1094 |
| | | (4)* 1050 | 897 | 1226 | 1075 |
| | | (5)* 1052 | 899 | 1236 | |

* Pulse number

24

Figure 6. Experimental Vs. Calculated Thermal Profiles

TABLE VIII

## CALCULATED CENTERLINE MASS DEPOSITION RATES

| ENGINE CONDITION | DEPOSITION RATES AT QCM (g/cm$^2$/sec) | | | |
|---|---|---|---|---|
| | Total $\times 10^7$ | $NH_3$ $\times 10^7$ | $H_2O$ $\times 10^9$ | $N_2H_4$ $\times 10^{10}$ |
| Baseline | 9.50 | 4.87 | 6.74 | 3.80 |
| Baseline (w/shield) | 9.33 | 4.79 | 6.67 | 3.76 |
| Short Pulse | 7.98 | 4.15 | 5.66 | 1.35 |
| Long Pulse | 8.81 | 4.00 | 6.23 | 8.79 |
| 70°F Catalyst Bed | 9.66 | 5.13 | 6.84 | 2.22 |
| 200°F Catalyst Bed | 9.56 | 5.07 | 6.79 | 2.39 |
| Baseline ($H_2O$ added) | 9.49 | 4.87 | 17.73 | 3.81 |

From Table VIII it can be observed that, although mass deposition from the short pulse and long pulse trains was predicted to be slightly less than that of the baseline case, total mass deposition does not vary a great deal with engine conditions. The fluctuations observed in the hydrazine flux are due almost entirely to fluctuations in hydrazine mass fraction (see Table IV). There is little difference in the deposition rates of water and ammonia for the different engine conditions, except of course for the "water added" case in which the water mass fraction is higher. The order of magnitude differences in the mass deposition rates of the three species are directly relatable to the order of magnitude differences in their mass fractions in the plume.

4.3 Comparisons with JPL Data: (Centerline)

Table IX presents a comparison between the predicted net deposition rates and the deposition rates measured by JPL.

From this table, it can be seen that, except for the 200°K case, the calculated net deposition rates are all, higher than the rates measured by JPL. Both sets of data are consistent, however, in that deposition rate decreases with

# TABLE IX

## MEASURED VS CALCULATED CENTERLINE DEPOSITION RATES AT QCM

NET DEPOSITION RATE (g/cm$^2$ - sec)

| ENGINE CONDITIONS | 106°K (x 10$^8$) | | 144°K (x 10$^?$) | | 172°K (x 10$^{10}$) | | 200°K (x 10$^{11}$) | |
|---|---|---|---|---|---|---|---|---|
| | JPL | CONTAM | JPL | CONTAM | JPL | CONTAM | JPL | CONTAM |
| Baseline | 7.54 | 39.7 | 2.89 | 6.98 | 1.22 | 3.77 | -- | -- |
| Baseline w/shield | -- | -- | 4.01 | 6.87 | 0.78 | 1.30 | 3.27 | 0 |
| Baseline (aged) | -- | -- | 1.50 | 6.98 | 1.11 | 3.77 | 6.02 | 0 |
| Short Pulse | -- | -- | 2.07 | 5.69 | 0.33 | 1.30 | 0 | -- |
| Long Pulse | -- | -- | 2.58 | 6.93 | 1.13 | 8.74 | -- | -- |
| 294° Cat Bed | -- | -- | -- | -- | 1.04 | 2.17 | -- | -- |
| 367° Cat Bed | -- | -- | -- | -- | 1.22 | 2.34 | -- | -- |
| Baseline (water added) | -- | -- | 4.39 | 17.70 | 1.14 | 3.77 | 0.98 | 0 |

increasing temperature. This is to be expected since the evaporation rate is an extremely strong function of temperature. Figure 7 is a plot of the predicted deposition vs. temperature for the various cases (the baseline with shield and the $294^{\circ}$ K catalyst bed conditions were not plotted because of their similarity with other cases). An examination of Figure 7 indicates discrete plateau regions where the predicted flux is constant over a range of temperatures. In other regions, the balance between deposition and evaporation is such that a small change in temperature results in a substantial change in net deposition rate. By considering each of these areas, one can get an excellent feel for what the predicted results mean. Above $190^{\circ}K$ no net deposition is predicted for any case. This is because the evaporation rate of all the species is higher at this temperature than any of the deposition rates. JPL did measure some deposition rates, but this may well be a species other than the three considered. Compounds from the carbonaceous impurities, especially aniline, are quite possible.

As the surface temperature is lowered from $190^{\circ}$ to $175^{\circ}K$, the evaporation rate and deposition rate of the hydrazine become balanced. The plateau region between $160^{\circ}$ and $175^{\circ}K$ is thus the temperature where all of the hydrazine in the flow which hits the crystal is expected to stick. The evaporation rates of water and ammonia at these temperatures still exceed their deposition rates. In general the predictions at $172^{\circ}K$ are from two to eight times higher than the data. If one considers the averaging techniques used to calculate hydrazine flux, and the small quantities of hydrazine predicted by the model, the lack of good agreement in the "all hydrazine" region is not surprising.

As the temperature of the surface is lowered below $160^{\circ}K$, the water evaporation rate quickly becomes comparable to the water deposition rate. Since there is much more water in the flow than there is hydrazine, a sharp increase in deposition is observed. At $150^{\circ}K$, the water deposition rate is much larger than the evaporation rate, and another temperature insensitive plateau region is reached. Between $110^{\circ}K$ and $145^{\circ}K$, all the water and hydrazine which hits the QCM is predicted to stick. At $144^{\circ}K$, the model predictions are still higher
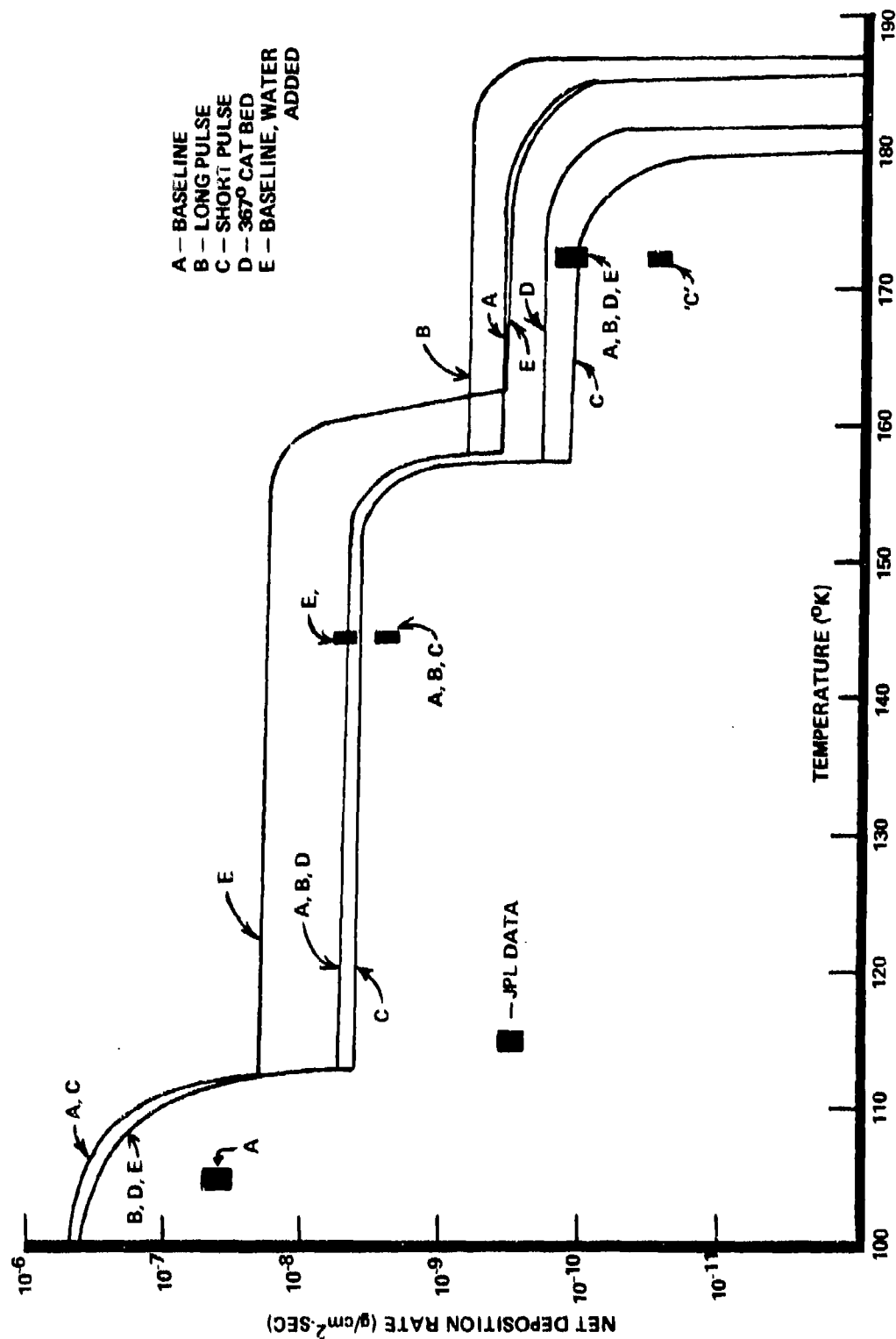
28

Figure 7. Net Deposition Rate Vs. Temperature

than the JPL data, but only by a factor of three or four. Ironically, one of the worst cases for agreement is the water added case.

Near $112^{\circ}$K the ammonia begins to deposit. Since ammonia is present in the largest quantity of the three species, once again there is a sharp rise in the net deposition curve. For the single $106^{\circ}$K comparison, the predicted value was a factor of five higher than the data. The results at this temperature are thus consistent with the other data.

### 4.4 Off-Centerline Mass Deposition Rates

Table X shows a comparison between CONTAM predicted mass fluxes for the centerline and the streamline that contains 99.99% of the mass between it and the centerline. These mass fluxes have been divided by the distance to the QCM squared (see Appendix A) but have not been adjusted for angle from the center-line. Unfortunately, as indicated in section 3.3, it was difficult to ascertain the angle at which a given streamline would impinge upon the QCM surface.

### TABLE X

### COMPARISON OF MASS FLUX ALONG CONTAM STREAMLINE

| ENGINE CONDITION | MASS DEPOSITION RATES AT QCM $(g/cm^2/sec)(\times 10^{-7})$ | | |
|---|---|---|---|
| | Centerline | 99.99% Streamline | Ratio |
| Baseline | 9.50 | 19.7 | 2.07 |
| Short Pulse | 7.98 | 7.77 | .97 |
| Long Pulse | 8.81 | 9.07 | 1.02 |
| $70^{\circ}$F Cat Bed | 9.66 | 8.03 | .83 |
| $200^{\circ}$F Cat Bed | 9.56 | 7.62 | .79 |

The 99.99% mass fluxes can be converted to net deposition rate (by subtracting the evaporation rate of each species) and then adjusted to the QCM off-centerline angle $\theta$ (multiplying by $\cos^2 \theta$). Table XI presents a comparison between these adjusted values and JPL's measurements.

30

## TABLE XI

## OFF-CENTERLINE MASS FLUX COMPARISONS[+]

Mass deposition (g/cm² - sec)

| | (x10⁹) 144°K | | | | (x10¹⁰) 172°K | | | |
|---|---|---|---|---|---|---|---|---|
| QCM ANGLE | 15° | | 30° | | 15° | | 30° | |
| Engine Condition | JPL | CONTAM* | JPL | CONTAM* | JPL | CONTAM* | JPL | CONTAM* |
| Baseline | 2.48 | 13.6 | .389 | 10.8 | .301 | 7.36 | .107 | 5.88 |
| Short Pulse | 1.80 | 5.06 | .189 | 4.04 | .122 | 1.24 | .017 | .97 |
| Long Pulse | 2.01 | 6.71 | .225 | 4.51 | .286 | 8.46 | -- | -- |
| 70°F Cat Bed | -- | -- | -- | -- | .131 | 1.72 | .0176 | 1.38 |
| 200°F Cat Bed | -- | -- | -- | -- | .285 | 1.78 | 0.179 | 1.43 |

+ See text for Calculation and interpretation

* 99.99% Streamline

In all cases the 99.99% streamline over estimates the deposition observed by JPL. In fact, if this streamline were considered to be at $70^O$, the maximum Prandtl-Meyer expansion angle that could be used, the predicted deposition is still higher than the JPL $15^O$ measurements. This example indicates that MULTRAN predicts the mass to be concentrated in too small an angle and points out a serious deficiency in the code.

# 5.0 DISCUSSION OF RESULTS

From the results of Table IX, it can readily be seen that the CONTAM model coupled with simple evaporation rate calculations predicts centerline mass deposition in excess of those measured by JPL. Such overprediction can occur as a result of either an overestimation of the mass flux arriving at the surface, an underestimation of the evaporation rate, or a combination of both these phenomena. JPL data was taken only once every twelve pulses, and thus deposition and evaporation could not be separated experimentally. However, in this section, these sources of error will be uncoupled as much as possible in order to evaluate the individual routines and analysis steps used in this effort. Appendix A presents a sample calculation which should be helpful in following the interactions of the various model predictions.

## 5.1 Deposition Rate Predictions Errors

Although the deposition rate predicted by CONTAM is made up of two values, the mass flux from the engine and the mass fraction of the individual species, it is possible to separate these using the calculations for the same engine conditions as a function of QCM temperature. From Figure 7 it can be seen that there are distinct temperature regions in which one can predict which of the three species considered will deposit. The order of magnitude changes predicted by CONTAM for the 106, 144, and 172°K QCM temperature were substantiated by the JPL data. Thus, one can postulate with some certainty that at 172°K only hydrazine will deposit, at 144°K only water and hydrazine, and at 106°K, water, hydrazine, and ammonia. Furthermore, because of the differences in mass fractions for the three species, the deposition at 106°K is principally ammonia, and at 144°K principally water. Since the mass fraction of water in the propellant is known with reasonable accuracy, one can use the 144°K crystal temperature to evaluate the mass flux predicted. At this temperature, CONTAM overpredicts the JPL data by 1.5 to almost 5.0. Similarly, although the $NH_3$ mass fractions of around 0.5 are what one would expect, the CONTAM mass flux is again overpredicted by 5.0 at 106°K, the temperature at which one expects

33

the deposit to be mostly $NH_3$. Since mass flux is proportional to $T^{-1/2}$ (ie., $\rho V \sim (T^{-1})(T^{1/2}) \sim T^{-1/2}$ ), uncertainties in temperature predictions cannot reasonably explain these large factors. In section 4.4 it was shown that MULTRAN incompletely expands the plume. Thus, this routine would be expected to concentrate the mass near the centerline. Therefore MULTRAN is the most likely cause of the overpredictions of the mass deposition rate.

## 5.2 Evaporation Rate Prediction Errors

As in the mass deposition discussion, there are two possible error sources for the evaporation rate predictions: the equations used to calculate the vapor pressures and the evaporation rate, and the surface temperature used in the calculation. There is little question that the $NH_3$ and $N_2H_4$ vapor pressure equations are not extremely accurate. However, the strong function of temperature on vapor pressure makes the temperature used the most critical aspect. Likewise, the temperature effect all but overrides any errors in the evaporation rate equation itself. It is quite likely that, due to the kinetic energy impacted to the surface by the impacting gases, the effective temperature for evaporation would be higher than that recorded by JPL. This higher temperature would cause evaporation rates to be greater than predicted. If one examines Figure 7 it can be observed that the JPL data are taken quite close to the break points in the curve, those points where evaporation rate balances mass flux. Higher temperature of evaporation would shift the JPL data to the right, thus providing better agreement between experimental and calculated net deposition.

## 5.3 Evaluation of CONTAM Routines and Procedures

Based on the above discussion (5.1), each routine and analysis technique will be assessed.

The N2H4 routine predicts the chamber conditions which are to be used by MULTRAN and the mass fractions used by KINCON. With the exception of hydrazine, the mass fractions of the species are predicted accurately. The temperature determined by N2H4 will have an effect on the results and there were some problems in this calculation (see section 3.2). However, this effect

34

will be of a second order. The chamber pressure predicted by N2H4 agreed well with the JPL data. The N2H4 code is not the weak link in the chain. Since N2H4 is based on a NASA performance code verified during development, this agreement is to be expected.

The MULTRAN routine generates the streamlines for use in KINCON. The lack of a proper plume expansion in MULTRAN is probably a major reason for overprediction along the centerline.

The KINCON code appeared to perform well. No serious irregularities were encountered. However, no kinetics or condensation were employed, and so KINCON was not tested to its fullest.

The use of evaporation rates to adjust the deposition rates worked very well. While better $NH_3$ and $N_2H_4$ vapor pressure data would be useful, the order of magnitude agreement indicates that the technique is acceptable. The actual temperature of the surface plays a significant part in the evaporation rate, and an accurate knowledge of this information is essential to proper net deposition rate calculations. Errors in this value are another major source of overprediction.

# 6.0 CONCLUSIONS

As a result of the comparisons performed on this effort, the following conclusions as to the effectiveness of the CONTAM code to predict net deposition can be made:

1. The subroutines of the CONTAM code (N2H4, MULTRAN, and KINCON) coupled with a simple evaporation rate model, predicted net deposition rates along the plume centerline which were consistently higher (by factors of 2 to 8) than the measured rates. Thus, the use of CONTAM would lead to overprediction of the centerline deposition rates. The CONTAM predictions did follow the same QCM temperature trends as the JPL data, however, and could be used to make order of magnitude predictions -- again for the centerline only.

2. MULTRAN does not properly handle the expansion of the plume. The lack of a proper boundary layer treatment is a known deficiency in the code and is most likely responsible for the overprediction along the centerline. Use of the CONTAM code should give conservative estimates along the centerline, but care should be taken when calculating off centerline deposition. Unfortunately, these regions are by far the most critical regions for contamination considerations.

3. The N2H4 routine appeared to calculate the mass fractions, with the exception of hydrazine, and temperatures adequately enough for input into MULTRAN and KINCON. The hydrazine prediction would be important only in the case of surfaces between $\sim 144^\circ$ and $\sim 180^\circ K$ or if the hydrazine flux was abnormally high, as with an aged thruster. While the lack of an aging mode is a serious consideration for performance, it is only of minor importance for most contamination assessments.

4. The KINCON model was not assessed in its full options, (condensation and with kinetics). Condensation may play a critical part of the hydrazine plume; kinetics do not. As used, the KINCON model appeared to yield consistent and reasonable results.

5. The use of an evaporation rate model to calculate net deposition appears adequate. The strong effect of temperature on evaporation points out the need to

36

know quite accurately the temperature of the surface on which one is trying to predict deposition. This effect raises some questions regarding the use of QCM temperature to characterize the evaporation rate, since the temperature of the deposit may be higher due to the kinetic energy of the impinging gases.

37

# 7.0 FUTURE STUDIES

Based on the results of the analysis, a great many questions have surfaced concerning the modeling of plume contamination from hydrazine thrusters. Because the JPL measurements were made only every 120 seconds, the effects of a single pulse and the off-time could not be separated. These measurements are extremely critical during the initial operation of the thruster. Also, such measurements would help determine the quantitative acceptability of the evaporation rate and the averaging techniques.

To answer these questions, a test program is being conducted at the Arnold Engineering and Development Center (AEDC). Using the same thruster tested at JPL, AEDC will measure composition and densities of the plume as well as net deposition as a function of time. Deposition rate measurements will be made on a pulse by pulse basis so that the effects of deposition and evaporation can be separated. Off-axis and backflow measurements of the mass deposition rates for the plume expansion are also being made. In addition to this program, the AFRPL will be conducting an analytical program to improve the CONTAM model, as identified in this study, and to compare predictions from the improved code with the AEDC test data.

For contamination predictions alone it is doubtful that additional engine modeling would be in order. For performance predictions, however, there is vast room for improvement. The AFRPL is contemplating a program to improve existing codes for performance and life prediction. The model would be useful to contamination prediction for those conditions in which hydrazine flux is important. Also, with a model which could predict engine aging (which $N_2H_4$ currently can not); one would be able to assess whether hydrazine related contamination would be a problem anytime during the entire mission life of the thruster.

38

# APPENDIX A  SAMPLE CALCULATIONS

The purpose of this appendix is to present a sample calculation in order that one may follow the procedure used to calculate the net deposition predicted from the CONTAM code coupled with the simple evaporation model. The case used is that of the baseline case (Table A-I summarizes this case); references are to equations or Tables found in the text.

## TABLE A-I

### BASELINE CASE

Mass Fractions (From N2H4):

$NH_3$ = .51354

$N_2$ = .46365

$H_2$ = .01571

$N_2H_4$ = 4 x 10$^{-4}$

$H_2O$ = .0071

Duty Cycle: 0.1 sec on/10 sec off

Distance to QCM: 113.4 cm (centerline)

From the KINCON output, density and velocity as function of time can be obtained. These values are used in equation (1) to calculate a mass flux per unit area as a function of distance and then, using equation (2), a mass flux per unit solid angle. For the baseline case $\frac{d\dot{m}}{d\Omega}$ = .822 g/ster-sec   This value is then converted to a mass flux per unit area at the QCM by solving equation (2) for r = 113 4 cm.

$$\dot{m} = 6 \ 39 \times 10^{-5} \ g/cm^2 - sec$$

This value is the flux predicted to hit the QCM during the time when mass is being discharged from the thruster. The total buildup rate on the QCM has to

include the off time as well. Thus the value is adjusted by a ratio of the "on" time to the total time/pulse.

$$\dot{m} = 6.39 \times 10^{-5} \times \frac{0.15}{10.1} = 9.50 \times 10^{-7} \ \text{g/cm}^2 - \text{sec}$$

Note that 0.1 seconds is the on time for the pulse. However, 0.15 is used because the mass flow rate at times between 0.1 and 0.15 seconds was considered great enough to contribute to the deposition. If 0.1 was used, the average value of the properties would be higher, and thus this effect should be minimal. Dividing by 10.1 is critical, however, since the JPL measurements did not differentiate between on and off time.

To calculate the individual mass flux for each species, equation (3) is used. Table A-II presents the values for each species considered.

### TABLE A-II

### SPECIES DEPOSITION RATE

$NH_3 = 4.86 \times 10^{-7} \ \text{g/cm}^2 - \text{sec}$

$H_2O = 6.74 \times 10^{-9} \ \text{g/cm}^2 - \text{sec}$

$N_2H_4 = 3.80 \times 10^{-10} \ \text{g/cm}^2 - \text{sec}$

The values in Table A-II are the fluxes that would be expected to deposit on the crystal if there were no evaporation. The following tables present the results of the evaporation rate calculations.

### TABLE A-III

### VAPOR PRESSURE CALCULATIONS* (torr)

| Species | Temperature ($K^\circ$) | | | |
|---|---|---|---|---|
| | 106 | 144 | 172 | 200 |
| $NH_3$ (eq 5) | $4.15 \times 10^{-6}$ | $4.75 \times 10^{-2}$ | -- | -- |
| $H_2O$ (eq 6) | $2.02 \times 10^{-15}$ | $6.35 \times 10^{-9}$ | $5.90 \times 10^{-6}$ | $8.13 \times 10^{-4}$ |
| $N_2H_4$ (eq 7) | -- | $2.37 \times 10^{-17}$ | $1.0 \times 10^{-10}$ | $7.98 \times 10^{-7}$ |

* shown only for vapor pressure ($P_v$) of interest: $10^{-4} > P_v > 10^{-18}$

TABLE A-IV

EVAPORATION RATE CALCULATIONS * (eq 4) g/cm$^2$ - sec

| Species | Temperature ($^\circ$K) | | | |
|---------|------|------|------|------|
| | 106 | 144 | 172 | 200 |
| NH$_3$ | $9.70 \times 10^{-8}$ | $9.51 \times 10^{-4}$ | -- | -- |
| H$_2$O | $4.85 \times 10^{-17}$ | $1.31 \times 10^{-10}$ | $1.11 \times 10^{-7}$ | $1.42 \times 10^{-5}$ |
| N$_2$H$_4$ | -- | -- | $2.74 \times 10^{-12}$ | $1.86 \times 10^{-8}$ |

* Shown only for Evaporation rate (Ev) of interest: $10^{-4} > Ev > 10^{-17}$

By subtracting the evaporation rates (Table A-IV) from the deposition rates (Table A-III) the net deposition rates are obtained (Table A-V). Note that a negative value for a species represents no deposition. The total deposition rates (sum of the species) are then used to compare the CONTAM predictions to the JPL measurements.

TABLE A-V

NET DEPOSITION RATES  (g/cm$^2$ - sec)

| Species | Temperature ($^\circ$K) | | | |
|---------|------|------|------|------|
| | 106 | 144 | 172 | 200 |
| NH$_3$ | $3.90 \times 10^{-7}$ | 0 | 0 | 0 |
| H$_2$O | $6.74 \times 10^{-9}$ | $6.60 \times 10^{-9}$ | 0 | 0 |
| N$_2$H$_4$ | $3.80 \times 10^{-10}$ | $3.77 \times 10^{-10}$ | $3.79 \times 10^{-10}$ | 0 |
| TOTAL | $3.97 \times 10^{-7}$ | $6.98 \times 10^{-9}$ | $3.77 \times 10^{-10}$ | 0 |

# APPENDIX B

## NET DEPOSITION PREDICTIONS FOR HYDRAZINE THRUSTERS

This appendix presents a simple method for estimating deposition rates from hydrazine thrusters on spacecraft surfaces without implementation of the complex CONTAM code. The method is based on the results of the CONTAM evaluation, the JPL test data, generalizations regarding hydrazine thrusters, and empirical relationships between plume centerline and backflow mass flux. Whenever possible, conservative approximations are made, and thus, if this analysis indicates that deposition will occur, a more detailed analysis with the CONTAM code may be called for. One should be aware that these estimates are subject to many of the same qualifications described in the text for CONTAM.

In order to demonstrate the application of the technique discussed here, an estimate of deposition from a 5 lb$_f$ thruster for the NATO III Satellite will be carried out. A more detailed analysis of the deposition from this thruster has previously been done using the CONTAM Code,[11] and thus an evaluation of this technique is available. Appendix A should be used as a guide in following the subsequent analysis.

## Mass Flux Calculations

The initial step in analyzing the deposition from any thruster is to determine the mass flux from that thruster. While this mass flux is a function of many variables it should be approximately proportional to the mass flowrate. Since the Isp of hydrazine thrusters lies between 100 - 230 seconds, the flowrate will vary from thruster to thruster by no more than a factor of 2.3 times the thrust. For the 0.1 lb$_f$ engine, the mass flux ranged from .7→1.0 g/ster-sec. Using

---

(11) L. P. Davis and I. L. Witbracht, Thruster Contamination Predictions for NATO III Satellite, AFRPL-TR-75-67, December 1975.

1.0 g/ster-sec and the 2.3 factor, the following can be used to calculate the mass flux:

$$\left(\frac{d\dot{m}}{d\Omega}\right)_T = 2.3\left(\frac{1.0}{0.1}\right) F_T = 23\ F_T\ \text{g/sec-ster} \qquad (B-1)$$

where: $\left(\frac{d\dot{m}}{d\Omega}\right)_T$ = mass flux of thruster (g/sec-ster)

$F_T$ = Thrust of thruster ($lb_f$)

1.0/0.1 = ratio of mass flux of 0.1 $lb_f$ thruster to its thrust

2.3 = factor to account for low impulse of the shorter pulses.

## Mass Fraction Analysis

To convert total mass flux to that for individual species, the mass fraction of the species in the plume must be known. Since all hydrazine thrusters have similar performance parameters, the mass fractions of water, hydrazine, and ammonia can be estimated with reasonable accuracy. For water, its mass fraction in the propellant should be used; the highest permissable value for mono-propellant grade is .01. A typical mass fraction of 0.5 for $NH_3$ can be used. Typical hydrazine mass fractions range from $10^{-2}$ to $10^{-4}$. This value is by far the most difficult to generalize, since it depends greatly on duty cycle and catalyst bed age. For this analysis, $10^{-2}$ will be used.

One could extend the analysis to include the presence of other contaminants, aniline for example, but further analysis would necessitate a knowledge of the form and mass fraction of the species in the plume and, hence, will not be done here. Combining the value of the total mass flux (B-1) with the species mass fluxes gives mass deposition rates per solid angle for the three species considered as follows:

$$\left(\frac{d\dot{m}}{d\Omega}\right)_i = 23\ X_i\ F_T \qquad (B-2)$$

where: $\left(\frac{d\dot{m}}{d\Omega}\right)_i$ = mass flux per solid angle for species i

$X_i$ = mass fraction per species i (see Table B-I for suggested values)

## TABLE B-I

### SUGGESTED VALUES FOR SPECIES MASS FRACTIONS

| Species | Suggested Range | Used in Analysis |
|---------|-----------------|------------------|
| Hydrazine | $10^{-2} - 10^{-4}$ | .01 |
| $NH_3$ | 0. 5 | 0. 5 |
| Water | .005 - .01 | 0. 01 |
| Other | As determined by used | Not considered |

Estimation of Species Flux to Spacecraft Surface

There are four factors in converting the flux per solid angle (eq. B-2) to actual fluxes at the spacecraft surface: distance from the exit plane to the surface (r), the angle between the thruster centerline and a line drawn from the exit plane to the surface ($\theta$), the inclination of this surface with respect to that line ($\phi$), and the duty cycle to be considered. The geometric parameters are depicted in figure B-I.

The distance factor is simply taken into account by dividing $\left(\frac{d\dot{m}}{d\Omega}\right)_i$ for each species i by $r^2$. This converts the units to $g/cm^2$ - sec at that distance. The angular effect ($\theta$) cannot be calculated well, especially for the backflow region. Thus, the flux at any angle $\theta$ is estimated as a fraction of the centerline flux. Figure B-2 gives the function used to estimate this fraction. For relatively small values of $\theta$, the theoretical Hill and Draper approximation is used. For larger angles, the set of measurements performed at JPL on an expansion of nitrogen gas through a nozzle is used. [12] These measurements are now felt to be high in the backflow region [13], but their use represents a conservative estimate.

_____

(12) J. E. Chirivella, Molecular Flux Measurements in the Backflow Region of a Nozzle Plume, NASA Tech Memo 33-620, July 1973

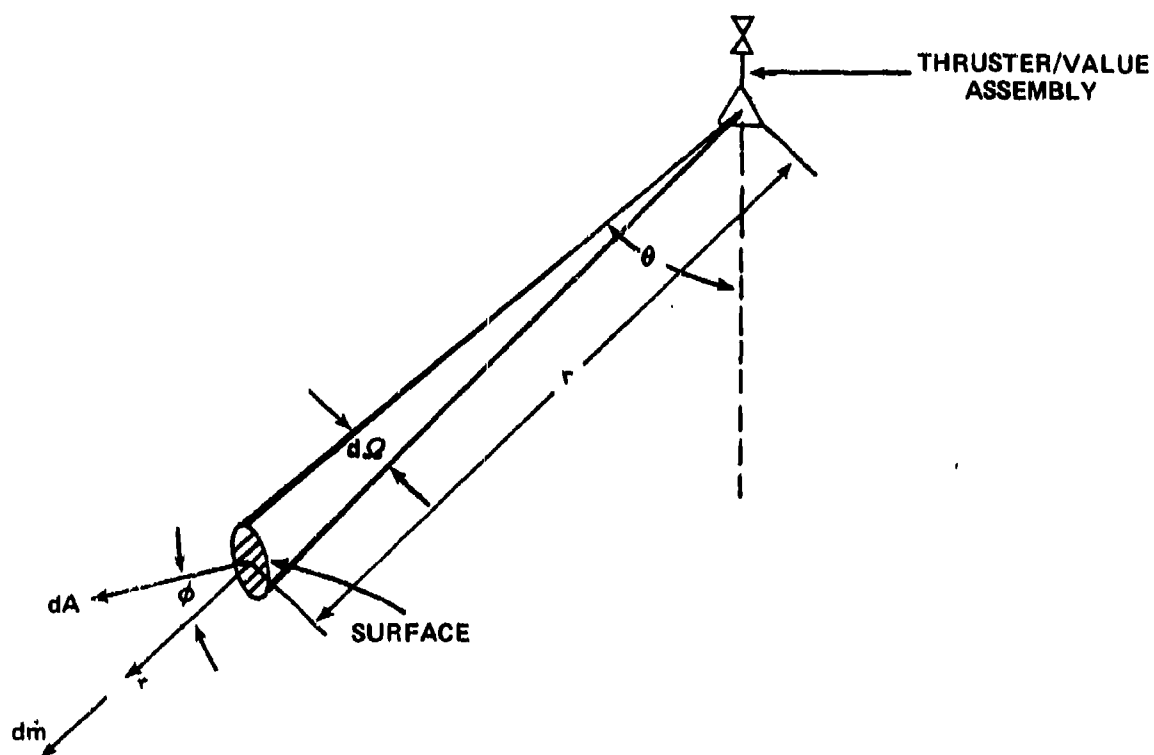(13) R. Passamaneck, Personal Communication

Figure B-1.  Geometrical Basis for Backflow Equations
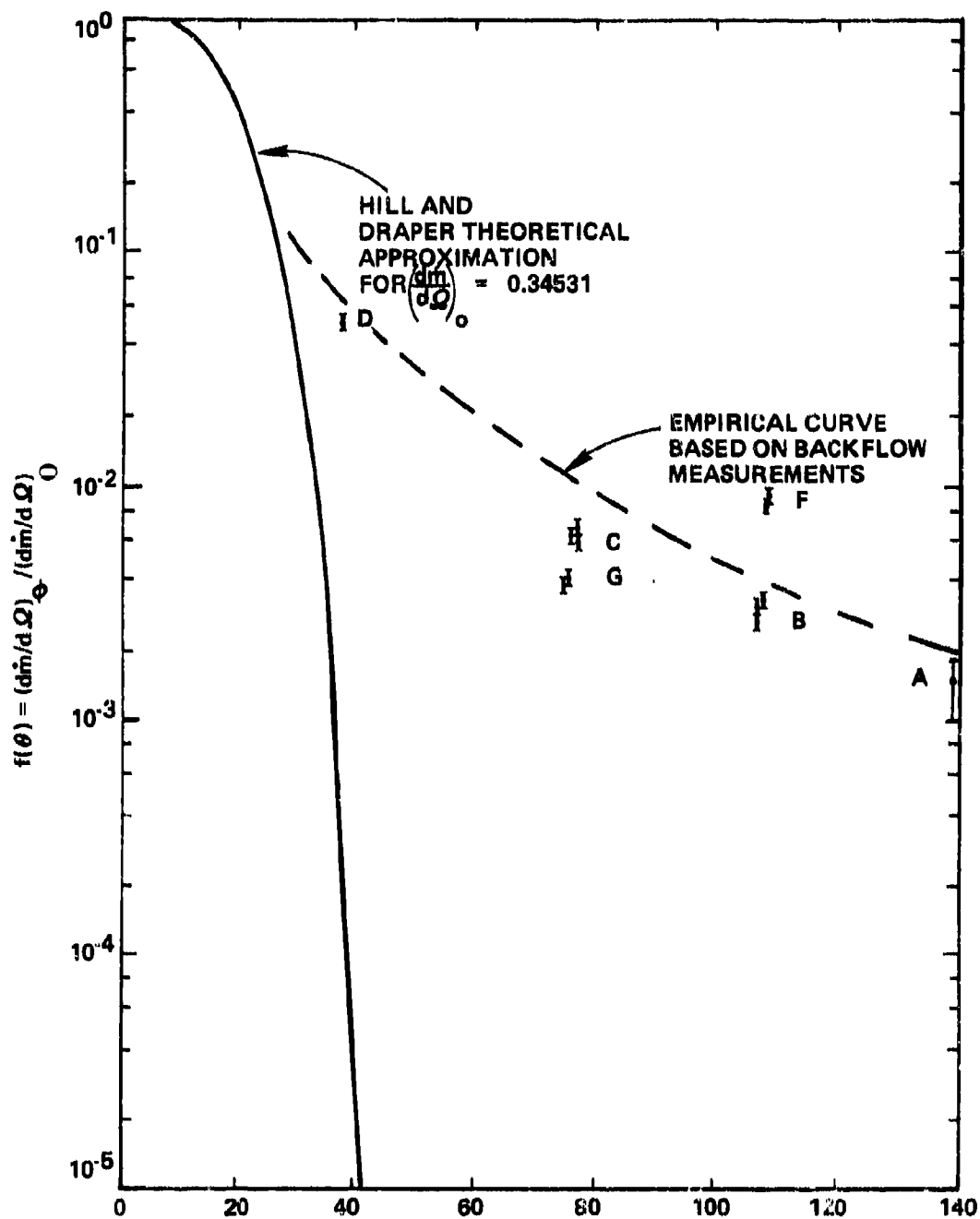(From Reference 12)

B-49

Figure B-2. Measured Values of $f(\theta)$ vs Backflow Angle $\theta$
(From Reference 12)

These were the same measurements used in the NATO III analysis. The surface inclination angle $\phi$ is taken into account with a $\cos \phi$ factor in the equation. The flux calculated so far is for the on-time of the thruster, which should be reduced by the percent of the duty cycle i. e. on-time/total pulse time.

These four factors result in the following equation for the flux through the surface:

$$\dot{m}_i = \frac{23 \; X_i \; F_T \; f(\theta) \; (DC)}{r^2 \cos \phi} \qquad \text{(B-3)}$$

where:  $\dot{m}_i$ is the flux through the surface in $g/cm^2$ - sec per species i

$f(\theta)$ = the emperical function of $\phi$ from Figure B-2

$\phi$ = the angle between the surface normal and a line joining the surface with the exit plane

$r$ = the distance between the exit plane and the surface in cm

DC = percent duty cycle, on-time/total pulse (dimensionless)

(DC = 1. 0 for steady state)

The fluxes calculated from equation B-3 represent the same fluxes as those of Table A-2, i. e. , the deposition rate of the species onto the surface. The net deposition rate at the surface is then calculated using the procedure's described in Appendix A. This value is the average deposition rate during a pulse (both on and off) and should be multiplied by the time of pulsing to yield total net deposition. Since evaporation is taking place continually, that rate may then be applied to the off time to determine the length of time for which there will be deposits on the surface.

Sample Case

The procedures described above will be used to assess the net deposition rate from a 5 $lb_f$ thruster used on the NATO III Satellite. The parameters to be used are described on Table B-II.

## TABLE B-II

### PARAMETERS FOR SAMPLE CASE

| Parameter | Nomenclature | Value |
|---|---|---|
| Percent Duty Cycle (on/total) | DC | .150 (.09 on/.511) |
| Total Pulse Time | $t_p$ | .601 |
| Surface Angle | $\phi$ | 60° |
| Distance to surface | r | 30 cm |
| Thrust | F | 5.0 $lb_f$ |
| Angle from centerline | $\theta$ | 120° |

From figure B-2, $f(120°) \approx 2 \times 10^{-3}$. Applying equation B-3 to this case using the mass fractions from table B-I yields the species deposition rates listed in Table B-III. That table also compares the results with those obtained for the NATO III thruster using CONTAM.

## TABLE B-III

### SPECIES DEPOSITION RATES ($g/cm^2$ - sec)

| Species | Estimation Technique | CONTAM |
|---|---|---|
| $NH_3$ | $3.82 \times 10^{-5}$ | $1.49 \times 10^{-5}$ |
| $H_2O$ | $7.65 \times 10^{-7}$ | $3.87 \times 10^{-7}$ |
| $N_2H_4$ | $7.65 \times 10^{-7}$ | $9.38 \times 10^{-8}$ |

It can be seen from table B-III that the technique predicts deposition rates which are within an order of magnitude of values predicted by CONTAM and conservative. Thus this technique should give good first estimate predictions. The next step is to use the evaporation rates from the surface to calculate the deposition expected as a result of a single pulse. Surface temperatures 216°K (-72°F) and 144°K (-200°F) will be used. The vapor pressure and evaporation rate equations discussed in Appendix A and the text were used to produce Table B-IV. By subtracting this rate from the deposition rate (Table B-III), estimated net deposition is obtained (Table B-V).

## TABLE B-IV

### SPECIES EVAPORATION RATES (g/cm-sec)

| Species | $216^{\circ}K$ | $144^{\circ}K$ |
|---|---|---|
| $NH_3$ | 461 | $9.51 \times 10^{-4}$ |
| $H_2O$ | $2.00 \times 10^{-4}$ | $1.31 \times 10^{-10}$ |
| $N_2H_4$ | $4.73 \times 10^{-7}$ | $6.5 \times 10^{-19}$ |

## TABLE B-V

### NET DEPOSITION RATES ($g/cm^2$ - sec)

| Species | $216^{\circ}K$ | $144^{\circ}K$ |
|---|---|---|
| $NH_3$ | 0 | 0 |
| $H_2O$ | 0 | $7.59 \times 10^{-7}$ |
| $N_2H_4$ | $2.92 \times 10^{-7}$ | $7.65 \times 10^{-7}$ |
| Total | $2.92 \times 10^{-7}$ | $1.52 \times 10^{-6}$ |

This analysis indicates that the net deposition during each second is $2.92 \times 10^{-7}$ $g/cm^2$ and $1.52 \times 10^{-6}$ $g/cm^2$ at $216^{\circ}K$ and $144^{\circ}K$ respectively. If the pulse train is 500 pulses long, then this deposition occurs for $0.601 \times 500$ or 300.5 seconds for a net mass buildup of $8.77 \times 10^{-5}$ g and $4.57 \times 10^{-4}$ g at $216^{\circ}K$ and $144^{\circ}K$ respectively. Using the appropriate evaporation rate will permit the determination of the length of time required to evaporate the deposition.

Graphical Calculations

A graphical method for estimating the net deposition can be performed using the following steps (sample calculation is shown on graphs).

1. Calculate the quantity $[DCF_T/r^2 \cos \phi]$ (for the sample above this value is $1.66 \times 10^{-3}$).

2. On Figure B-3, intersect a horizontal line from quantity (from 1) with a vertical line at the angle corresponding to the degrees off centerline ($120^{\circ}$ for the centerline). The mass flux is determined by the point of intersection. (In the sample case it is $1.1 \times 10^{-4}$ $g/cm^2$ - sec).
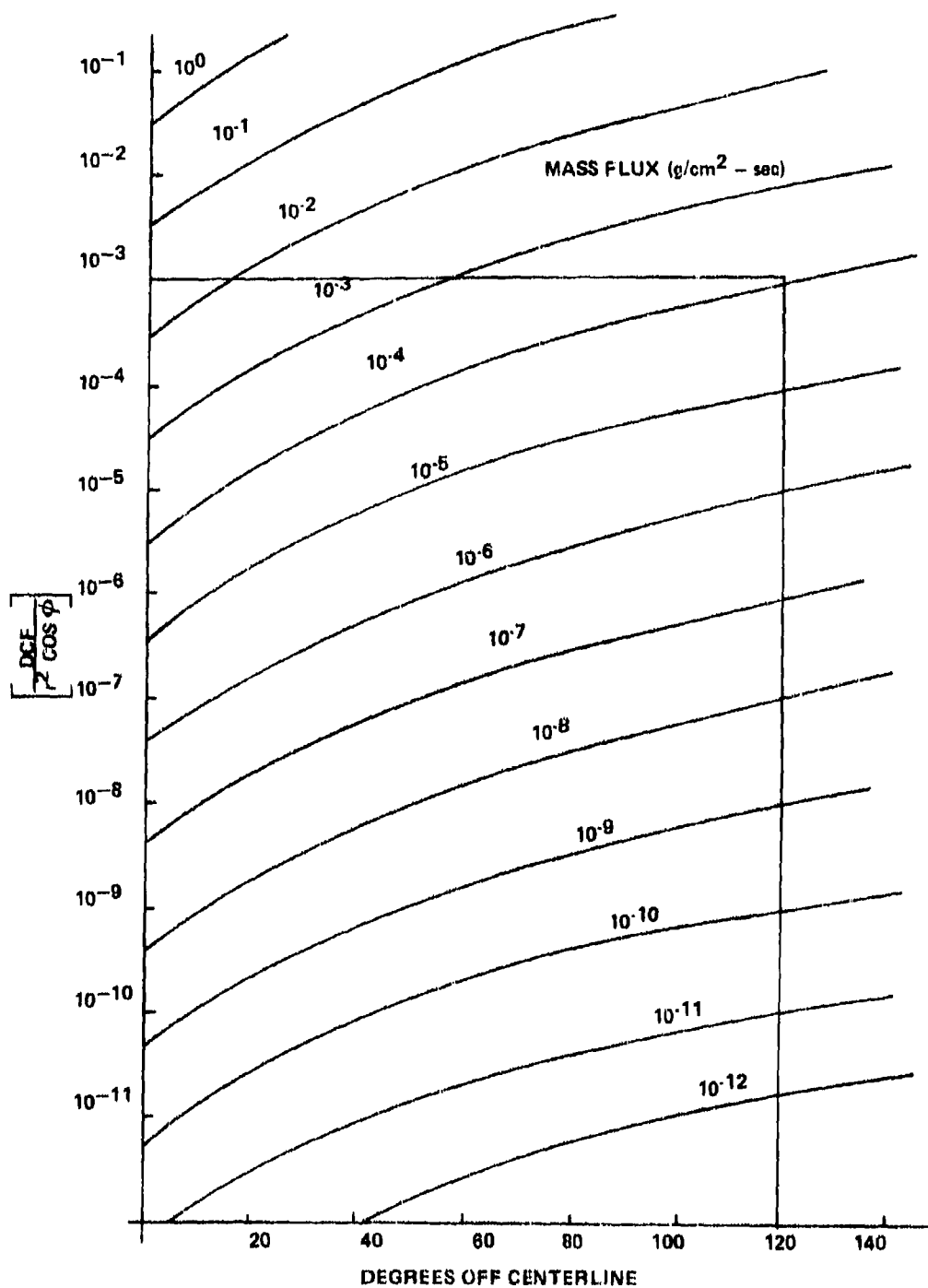
Figure B-3.

B-50

3. The mass flux should be multiplied by the mass fraction of each species considered. Figure B-4 contains suggested values.

4. The flux of each specie should be represented by a horizontal line on figure B-4 at the appropriate ordinate value.

5. The solid lines labled $NH_3$, $H_2O$, and $N_2H_4$ on Figure B-4 represent the evaporation rate of the species. Thus the difference between the intersection of a vertical line through a temperature with the horizontal line (from 4) and the solid line (evaporation rate) is the net deposition for that species. If this value is negative, there will be no deposition of that species. The temperature at which the horizontal line intersects the solid line is the temperature above which there will be no deposition of that species.

6. For the example at $216^{\circ}K$, only $N_2H_4$ is predicted to deposit with a rate of $10^{-6} - 3 \times 10^{-7} = 7 \times 10^{-7}$ (compared with $3 \times 10^{-7}$ for a rigorous calculation). For $144^{\circ}K$ all the hydrazine and water will deposit for a total of $2 \times 10^{-6}$ (compared with $1.5 \times 10^{-6}$ for the rigorous calculation). One can also deduce that no $NH_3$ will deposit until $128^{\circ}K$.
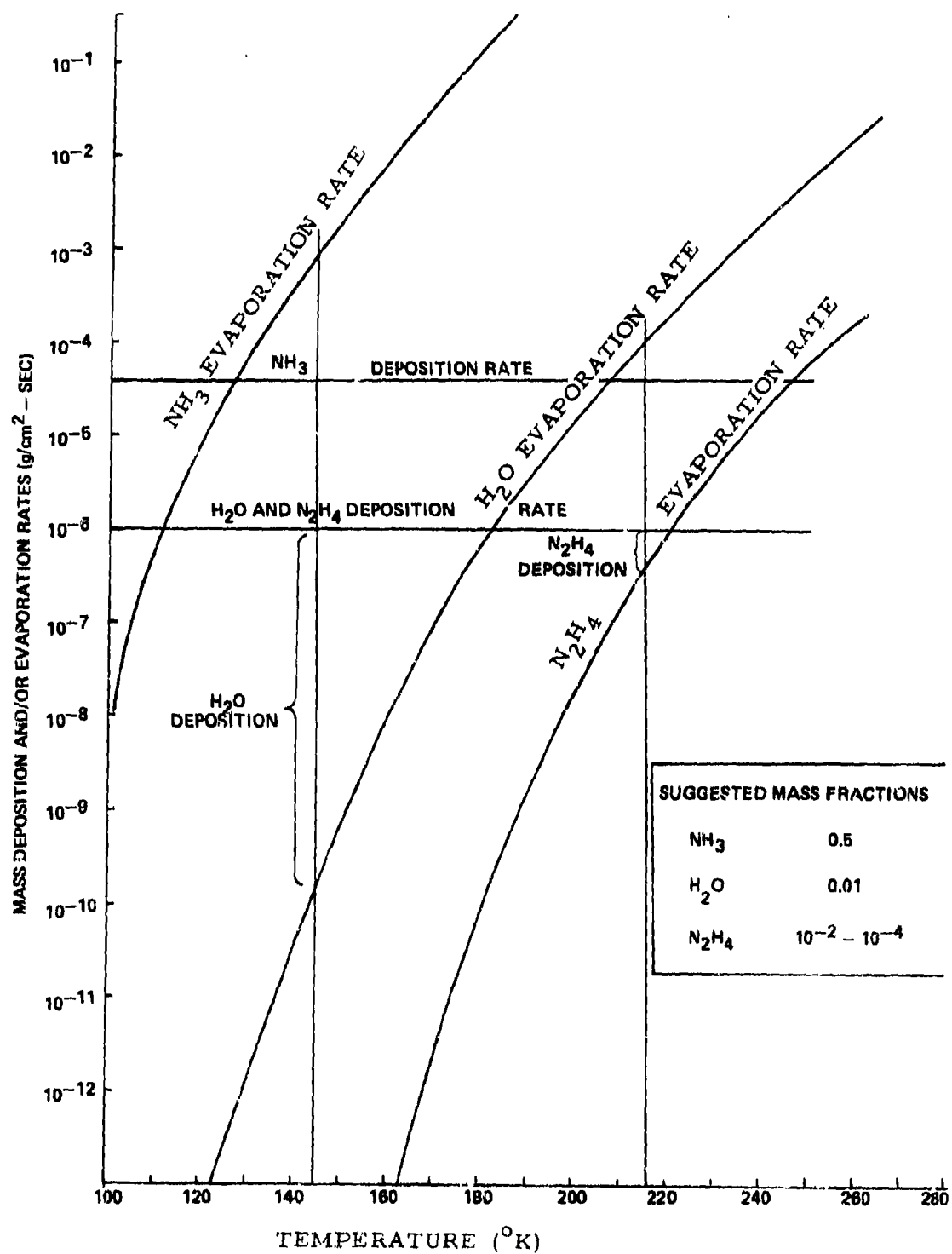
Figure B-4. Deposition and/or Evaporation Rates Vs Temp

# REFERENCES

(1) R. J. Hoffman, et. al., Plume Contamination Effects Prediction. The CONTAM Computer Program, Version II, AFRPL-TR-73-46, August 1973.

(2) R. Passamaneck and J. E. Chirivella, "Contamination Measurements for a 0.1 lb$_f$. Monopropellant Thruster," JANNAF Ninth Plume Technology Convention, February 1976.

(3) A. S. Kesten, Analytical Study of Catalytic Reactors for Hydrazine Decomposition. United Aircraft Research Laboratories Report G910461-24, Second Annual Progress Report, Contract NAS-7-458, May 1968.

(4) A. S. Kesten, Analytical Study of Catalytic Reactors for Hydrazine Decomposition. United Aircraft Research Laboratories Report H910461-38, Third Annual Progress Report, Contract NAS-7-458, May 1969.

(5) D. B. Smith, E. J. Smith, and A. S. Kesten, Analytical Study of Catalytic Reactors for Hydrazine Decomposition. United Aircraft Research Laboratories Report H910461-37, Computer Program Manual, Transient Model, May 1969.

(6) A. S. Kesten, Analytical Study of Catalytic Reactors for Hydrazine Decomposition. United Aircraft Research Laboratories Report F910461-12, First Annual Progress Report, Contract NAS-7-458, May 1967.

(7) D. B. Smith, E. J. Smith, and A. S. Kesten, Analytical Study of Catalytic Reactors for Hydrazine Decomposition. United Aircraft Research Laboratories Report G910461-30, Computer Programs Manual, One-Dimensional and Two-Dimensional Steady State Models, August 1968.

(8) R. J. Hoffman, et. al., Op. Cit., page 250.

(9) Handbook of Chemistry and Physics, The Chemical Rubber Company, Cleveland, Ohio, 1967-68 Edition.

(10) G. Jancso, et. al., J. Phys. Chem., 1970, 74 (15), 2984-9.

(11) L. P. Davis and I. L. Withracht, Thruster Contamination Predictions for NATO III Satellite, AFRPL-TR-75-67 December 1975.

(12) J. E. Chirivella, Molecular Flux Measurements in the Backflow Region of a Nozzle Plume, NASA Tech Memo 33-620, July 1973.

(13) R. Passamaneck, Personal Communication